Mineralogical Magazine, December 2016, Vol. 80(7), pp. 1161–1193

Magmatic, hydrothermal and subsolidus evolution of the agpaitic nepheline syenites of the Sushina Hill Complex, India: implications for the metamorphism of peralkaline syenites

A. Chakrabarty[1,*], R. H. Mitchell[2], M. Ren[3], P. K. Saha[1], S. Pal[1], K. L. Pruseth[4] and A. K. Sen[5]

[1] Department of Geology, Durgapur Government College, Durgapur 713214, West Bengal, India
[2] Department of Geology, Lakehead University, Thunder Bay, Ontario, Canada P7B 5E1
[3] Department of Geoscience, University of Nevada, Las Vegas, Nevada, USA
[4] Department of Geology and Geophysics, Indian Institute of Technology Kharagpur, Kharagpur 721302, India
[5] Department of Earth Sciences, Indian Institute of Technology Roorkee, Roorkee, Uttarakhand 247667, India

[*Received 23 March 2015; Accepted 10 November 2015; Associate Editor: Katharina Pfaff*]

ABSTRACT

The Proterozoic Sushina Hill Complex is the only agpaitic complex, reported from India and is characterized by a eudialyte-rinkite-bearing nepheline syenite. The complex is considered a 'metamorphosed agpaitic complex'. This study describes the mineral assemblages formed during successive stages of evolution from magmatic to hydrothermal stages and low-temperature subsolidus re-equilibration assemblage. The primary–late magmatic assemblage is characterized by albite, orthoclase, unaltered nepheline, zoned diopside–hedenbergite, rinkite, late magmatic eudialyte and magnesio-arfvedsonite formed at ~700°C with maximum a_{SiO_2} of 0.60. In contrast, a deuteric assemblage (400–348°C) is represented by aegirine–jadeite-rich clinopyroxene, post-magmatic eudialyte, sodalite, analcime and the decomposition assemblages formed after eudialyte with decreasing a_{SiO_2} (0.52–0.48). A further low-temperature subsolidus assemblage (≤250°C) represented by late-forming natrolite could be either related to regressive stages of metamorphism or a continuum of the subsolidus processes. Considering the *P*/*T* range of the greenschist – lower-amphibolite facies of metamorphism it is evident that the incorporation of a jadeite component within pyroxene is related to a subsolidus process between ~400°C and 348°C in a silica deficient environment. We emphasize that the deuteric fluid itself acted as an agent of metamorphism and the decomposition assemblage formed after eudialyte is retained even after metamorphism due to the convergence of subsolidus and metamorphic domains. The formation of jadeite-rich aegirine is not considered to result from metamorphism. Overall it is near-impossible to discern any *bona fide* metamorphic textures or mineral assemblages in these syenites which appear to preserve a relict mineralogy regardless of their occurrence in country rocks which have experienced greenschist – amphibolite facies metamorphism. The Sushina complex is very similar in this respect to the Norra Kärr complex (Sweden).

Keywords: metamorphosed agpaitic rocks, Sushina Hill, eudialyte, clinopyroxene, subsolidus alteration.

Introduction

Alkaline rocks are characterized by the modal or normative abundance of feldspathoids, alkali amphiboles and aegirine (Le Maitre, 2002; Marks *et al.*, 2011). On the basis of the peralkalinity index,

*E-mail: aniket_chakrabarty@rediffmail.com
DOI: 10.1180/minmag.2016.080.057

i.e. molar ratio of $Na_2O + K_2O$ relative to Al_2O_3, alkaline rocks are divided broadly into peralkaline [$Na_2O + K_2O > Al_2O_3$] and metaluminous [$(Na_2O + K_2O) < Al_2O_3 < (CaO + Na_2O + K_2O)$] types. Peralkaline rocks are well known as hosts for rare exotic minerals enriched in large ion lithophile elements (LILE): Na, K, Li; high-field-strength elements (HFSE): Ti, Zr, Nb, Ta, rare-earth elements (*REE*), U and Th (Ussing, 1912; Sørensen, 1992, 1997; Marks *et al.*, 2011). The term 'agpaitic' is restricted to a particular group of peralkaline nepheline syenites containing complex Na-Ca-Fe-Ti-Zr-*REE* silicates such as rinkite, eudialyte, mosandrite, låvenite etc. These minerals are termed the 'typomorphic' minerals of agpaitic systems. Some agpaitic syenites (e.g. Lovozero) enriched in Na are termed hyperagpaites (Khomyakov, 1995). In contrast, nepheline syenites which lack complex silicates and contain ilmenite, titanite and zircon are known as 'miaskitic' types. Agpaites are one of the most important variety of peralkaline feldspathoidal rocks owing to their potential to form economic mineral deposits (Ilímaussaq complex, Greenland; Lovozero and Khibina, Kola Peninsula, Russia; Pilansberg, South Africa; Mont Saint Hilaire, Canada; Tamazeght, Morocco) (Kogarko *et al.*, 1982; Mitchell and Liferovich, 2006; Marks *et al.*, 2011 and references therein; Schilling *et al.*, 2011*a*). Peralkaline syenites and granites (e.g. Straumsvola, Antarctica; Ascension Island; Strange Lake, Canada) are rarer than undersaturated peralkaline syenites. They usually lack titanite and contain eudialyte, elpidite, dalyite, vlasovite and aenigmatite (Harris and Rickard, 1987; Salvi and Williams-Jones, 1995).

Agpaitic rocks commonly experience metasomatism during their course of evolution from early-to-post-magmatic to hydrothermal stages (e.g. Pilansberg complex, South Africa, Mitchell and Liferovich, 2006; Thor Lake complex, Canada, Sheard *et al.*, 2012). The parent melt of the agpaitic rocks usually contains significant amounts of volatile species which induce metasomatic changes by their interaction with earlier crystallizing phases. Such phenomena eventually result in changes to both the mineralogical and textural features of the rock and are commonly termed autometasomatic/deuteric alteration.

In India, agpaitic rocks were not recognized until recently when an occurrence of eudialyte-bearing nepheline syenite gneiss from the Sushina Hill Complex at Purulia, West Bengal was reported by Chakrabarty (2009). This is the only known occurrence of agpaitic rock (*sensu stricto*) from the Indian subcontinent. The Sushina Hill Complex is composed of diverse undersaturated rocks including miaskitic and agpaitic nepheline syenite gneisses and albitite (Chakrabarty *et al.*, 2013). Mitchell and Chakrabarty (2012) reported compositionally different late-magmatic and hydrothermal Mn-rich eudialytes from the agpaitic units of the complex. Volumetrically, hydrothermal eudialyte dominates over the late-magmatic types. It is now well-established that the rocks of the complex have undergone extensive post-intrusion metasomatism together with multiple phases of metamorphism during Palaeo–Mesoproterozoic times (Chakrabarty and Sen, 2013). The majority of recent work on the peralkaline rocks of Sushina Hill have been restricted to describing eudialyte and rinkite and their decomposition to diverse *REE*-bearing phases such as cerianite-(Ce), hingganite-(Ce), catapleiite, hilairite (Chakrabarty *et al.*, 2011, 2013; Mitchell and Chakrabarty, 2011; Goswami and Basu, 2013), and little attention has been given to the major rock-forming minerals. Goswami and Basu (2013) reported a metamorphic assemblage of epidote, scapolite, piemontite and natrolite from these agpaitic gneisses and suggested the metamorphic grade was within greenschist-to-amphibolite facies. These authors also suggested that pure end-member compositions of nepheline, albite and orthoclase together with the development of gneissosity are suggestive of metamorphic origin for these agpaitic rocks.

Floor (1974) suggested that textural and mineralogical criteria are useful tools for distinguishing between alkaline rocks formed predominantly by igneous processes and those formed by metamorphic–metasomatic processes. In regions of moderate-to-high-grade metamorphism, such as experienced by the host rocks of Sushina Hill (India), Norra Kärr (Sweden) and Red Wine (Labrador, Canada) complexes, it is commonly found that igneous and metamorphic–metasomatic processes tend to converge making such distinctions difficult. The main objective of the present work is to distinguish between magmatic and metamorphic/metasomatic mineral parageneses of the Sushina Hill metamorphosed agpaites using mineralogical and textural criteria. Such a study is useful in delineating the paragenetic sequence of the magmatic-to-hydrothermal evolution of the agpaitic rocks and its relation to the subsequent metamorphism and deformation.

Geological setting

The Mesoproterozoic Sushina Hill complex (22° 57′N, 86°37′E) (~480 × 93 m^2) lies within Chandil

https://doi.org/10.1180/minmag.2016.080.057 Published online by Cambridge University Press

Formation of the North Singhbhum Mobile Belt, along a shear zone which is termed variously as the Northern Shear Zone or South Purulia Shear Zone (Saha, 1994). This WNW–ESE trending 100 km long discontinuous shear zone is located at the contact between the Chotanagpur Granitic Gneissic Complex in the north and the Chandil Formation in the south (Fig. 1*a*). This shear zone is believed to be an extension of the Central Indian Shear Zone (Rekha *et al.*, 2011). Alkaline intrusive rocks such as carbonatite, alkali-pyroxenite and nepheline syenite occur along the Northern Shear Zone (Basu 1993; Chakrabarty *et al.*, 2009, 2011, 2012; Chakrabarty and Sen, 2010, 2013; Mitchell and Chakrabarty, 2012). The Sushina Hill complex is composed of diverse undersaturated syenite gneisses within country rocks consisting of sodic-schists, phyllites and amphibolites. Two varieties of nepheline syenite gneiss namely, eudialyte nepheline gneiss (agpaitic) and miaskitic nepheline gneiss, have been recognized at Sushina Hill (Fig. 1*b*) together with a large albitite body (Chakrabarty, 2009). The miaskitic syenite is considered to be the oldest unit of the complex with an emplacement age of *c*. 1.51 Ga (Chakrabarty, 2009; Chakrabarty *et al.*, 2013). A similar age (*c*. 1.55 Ga) is also considered as the emplacement age of the carbonatite and anorthosite situated at the western and eastern extremities along the Northern Shear Zone (Chatterjee *et al.*, 2008; Chakrabarty and Sen, 2013).

The Sushina agpaitic gneisses, are characterized by the presence of the typomorphic minerals eudialyte and rinkite (Mitchell and Chakrabarty, 2012; Chakrabarty *et al.*, 2013). These occur together with albite (~45–50 modal%), orthoclase (~20–25 modal%), nepheline (~10–15 modal%), aegirine (~8–10 modal%) and arfvedsonite (<1 modal%). The gneiss is characterized by modal layering resulting from variations in the proportions of nepheline, feldspar and ferromagnesian minerals. The mafic minerals coalesce and cluster, giving rise to an incipient gneissic texture as well as a 'knotted' or 'mottled' appearance. Various textural features such as unusually elongated albite, nepheline and pyroxene along the gneissic trend, ovoid nature of some felsic minerals with their long axes parallel to the gneissic trend are suggestive of a metamorphic overprint on the precursor eudialyte syenite (Goswami and Basu, 2013). However, it must be noted that similar textural features found in the Norra Kärr agpaitic complex have been attributed entirely to magmatic processes (Adamson, 1944; von Eckermann, 1968). Similar textures are found in lujavrites from the Ilímaussaq complex which has not been subjected to any metamorphism and thus are considered as primary textural features (Ratschbacher *et al.*, 2015). Koark (1960, 1968) opined that some features at Norra Kärr, such as the development of the gneissosity, shearing, and folding are the result of the metamorphic overprinting on an igneous lithology. The presence of an albitized zone around the agpaitic rocks of the Sushina Hill complex is also similar to the fenitized zone found at the contact between the catapleiite syenite (grennaite) and Växjö granite at Norra Kärr (Sjöqvist *et al.*, 2013). However, unlike the Norra Kärr rocks none of the Sushina agpaites are schistose. The emplacement age of the Sushina nepheline syenite is not well constrained. A recent study of the post-magmatic eudialyte by the Rb-Sr, Sm-Nd and Lu-Hf methods, confirms that eudialyte precipitation from the deuteric fluid occurred at *c*. 1.30 Ga and therefore the emplacement age of the host agpaitic syenite is considered to be older than 1.30 Ga (authors' unpublished data).

It is now well established that the rocks of both Chotanagpur Granitic Gneissic Complex as well as the North Singhbhum Mobile Belt, experienced multiple phases of metamorphism accompanied by distinctive deformational events between *c*. 1.87 and 0.78 Ga (Maji *et al.*, 2008; Rekha *et al.*, 2011; Sanyal and Sengupta, 2012). The earliest metamorphic event is recorded within the granulite enclaves in Chotanagpur Granitic Gneissic Complex at *c*. 1.87 Ga (>900°C at *c*. 5–8 kbar). This was followed by felsic magmatism and contemporaneous metamorphism at *c*. 1.66–1.55 Ga. Alkaline magmatism (carbonatite and nepheline syenite) was accompanied by the intrusion of a suite of anorthosite and porphyritic granitoids at *c*. 1.55–1.51 Ga. These experienced greenschist-to-amphibolite facies metamorphism (*c*. 700 ± 50°C, 6.5 ± 1 kbar) between 1.20 and 0.93 Ga. A final phase of metamorphism (600–750°C at 7 ± 1 kbar) related to defragmentation of the Rodinia supercontinent affected the entire eastern margin of the Indian subcontinent at ~0.87–0.78 Ga, and resulted in the formation of the Eastern Indian Tectonic Zone (Chatterjee *et al.*, 2010). This last metamorphic event is wide-spread both within the Chotanagpur Granitic Gneissic Complex and North Singhbhum Mobile Belt (Chatterjee and Ghose, 2011; Rekha *et al.*, 2011). Although, the detailed metamorphic history of the Sushina Hill complex is yet to be investigated systematically, available data suggests that the rocks

https://doi.org/10.1180/minmag.2016.080.057 Published online by Cambridge University Press

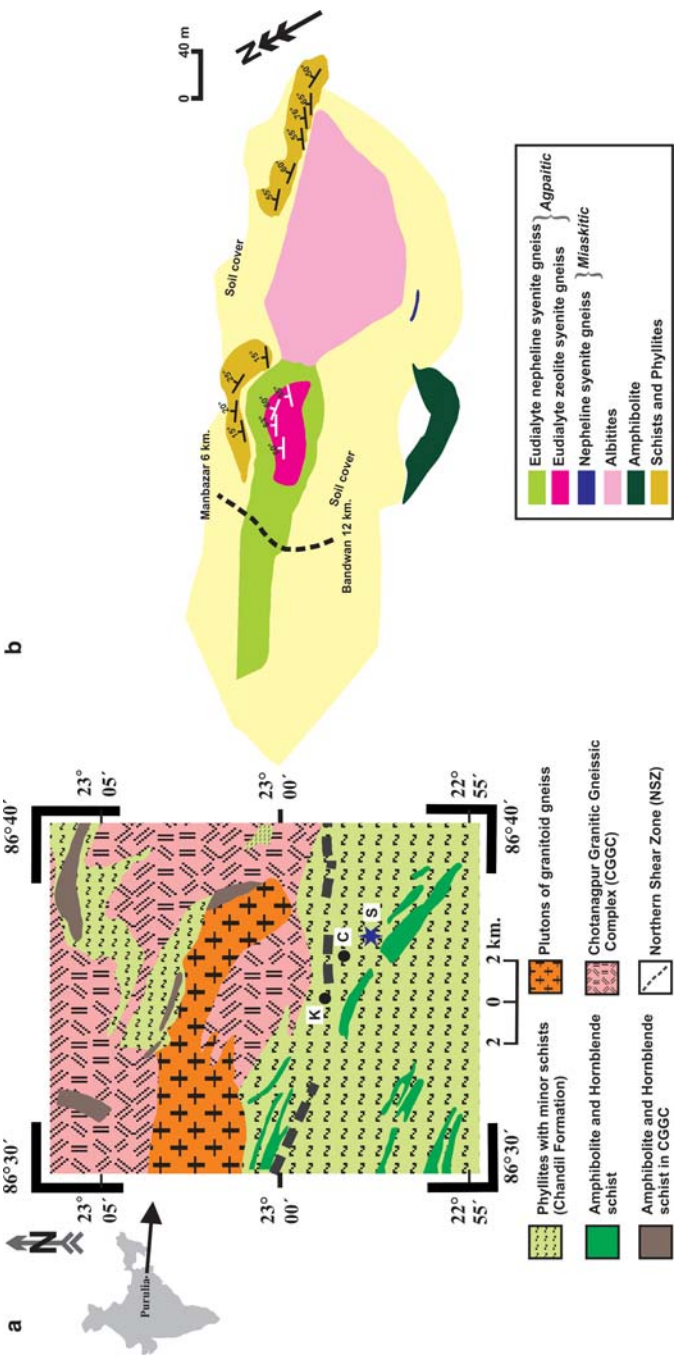

FIG. 1. (*a*) Regional geological map of part of the Purulia–Chotanagpur area along the Northern Shear Zone. The area investigated is located at S (Sushina) and marked by the blue star. K (Kutni) and C (Chirugora) are localities of carbonatite and apatite-magnetite occurrences. (*b*) Detailed lithological map of the Sushina Hill complex showing the disposition of different lithological units present within the complex.

https://doi.org/10.1180/minmag.2016.080.057 Published online by Cambridge University Press

of the complex experienced metamorphism at *c*. 1.20 and 0.87 Ga, respectively (Chakrabarty, 2009; Chakrabarty and Sen, 2013).

Analytical methods

Mineral compositions were determined on polished thin sections using a JXA-8900 SuperProbe and CAMECA SX-100 electron microprobe operated in wavelength-dispersive mode at the Electron Microanalysis and Imaging Laboratory (EMIL), University of Nevada, Las Vegas (UNLV), USA and Institute Instrumentation Centre (IIC), IIT Roorkee, India, respectively. Polished sections were examined by optical microscopy to identify target areas for analyses. Selection of analytical sites was also guided by back-scattered electron imagery. For a majority of the silicate minerals such as feldspar, clinopyroxene, amphibole, garnet, nepheline and sodalite, we used a beam current of 15 nA and an acceleration voltage of 15 kV. Peak counting times were 16–20 s for major elements and 30–60 s for minor elements. For eudialyte, a beam current of 20 nA and an acceleration voltage of 20 kV were used as described by Pfaff *et al.* (2010). The peak counting times were generally between 16 and 120 s, depending on the abundance of the respective element. Background counting times were kept at half of the peak counting times for all analyses. Special attention was given to avoid Na migration under the electron beam during analyses of feldspar, nepheline, eudialyte, sodalite and zeolite-group minerals. This was achieved by first analysing Na with a defocused beam of 10 μm or where possible 20 μm and with peak-counting time not exceeding 10 and 5 s on the background. The following well-characterized minerals and synthetic standards were used: Na (Na*Kα:* jadeite); fayalite (Fe*Kα*); wollastonite (Si*Kα*, Ca*Kα*); olivine (Mg*Kα*); sanidine (K*Kα*); zircon (Zr*Lα*); titanite (Ti*Kα*); Nb (Nb*Lα*); Al_2O_3 (Al*Kα*); rhodonite (Mn*Kα*); BaF_2 (F*Kα*); *REE*-phosphates (*REE Lα* for La, Ce, Yb, Lu; *REE Lβ* for the remaining *REEs*); YPO_4 (Y*Lα*) and halite (Cl*Kα*). Peak overlaps between Fe and F; Nd and Zr; Ti and Hf and other *REE*s (Chakrabarty *et al.*, 2013) were corrected. Processing of the raw data was carried out with the internal ϕρZ correction method of JEOL (for JXA-8900) (Armstrong, 1991) and *PAP CAMECA* software (for CAMECA SX-100) (Pouchou and Pichoir, 1991). Analytical precision based on replicate analyses of standards has standard deviation <0.5 for major and <0.1 for minor elements. The method of Droop (1987) was used to recalculate the microprobe-obtained total Fe (as FeO wt.%) to Fe^{3+} and Fe^{2+} for clinopyroxenes, amphiboles and garnet.

Major primary silicates – paragenesis and compositions

Feldspar

Albite and orthoclase are the predominant felsic minerals in the agpaitic syenite gneiss. These form discrete crystals and primarily present as macrocrysts. However, albite (>45 modal%) is volumetrically more abundant than orthoclase (20–25 modal%). In places megacrystic albite (up to 1 cm) containing early-formed nepheline and clinopyroxene is well preserved. However, such megacrystic albite is commonly found to be extensively-altered by late-stage hydrothermal activity. Orthoclase crystals are also coarse grained (>250 μm) and present as macrocrysts and as granular crystals (Fig. 2*a*,*b*). The majority of the albite and orthoclase are typically subhedral and show hypidiomorphic interlocking textures demonstrating the plutonic character of the rock. Marginal granulation of the megacrystic albite, polygonal contacts between albite and orthoclase, and elongated-platy habit of the feldspars in some places is suggestive of post-crystallization deformation. These textural features are similar to those observed in the Norra Kärr catapleiite syenites (Fig. 2*c*,*d*), although cataclastic textures have not been observed at Sushina.

In terms of their composition both feldspars represent end-member albite and orthoclase, respectively with no anorthite component (Table 1). The presence of microcline at the margins of orthoclase macrocrysts and incipient development of cross-hatched twinning (Fig. 2*b*,*e*) indicates some re-equilibration has taken place at relatively lower temperatures. The rare presence of antiperthite in association with albite and orthoclase probably indicates that exsolution of orthoclase occurred during low-temperature alteration (Fig. 2*f*). In places twinned albite with subsequent conversion to antiperthite (Fig. 2*f*) is also observed.

Nepheline

Discrete crystals of subhedral-to-anhedral nepheline occur in two distinct textural modes. Early-formed unaltered nepheline (Ne-I) occurs as inclusions

https://doi.org/10.1180/minmag.2016.080.057 Published online by Cambridge University Press

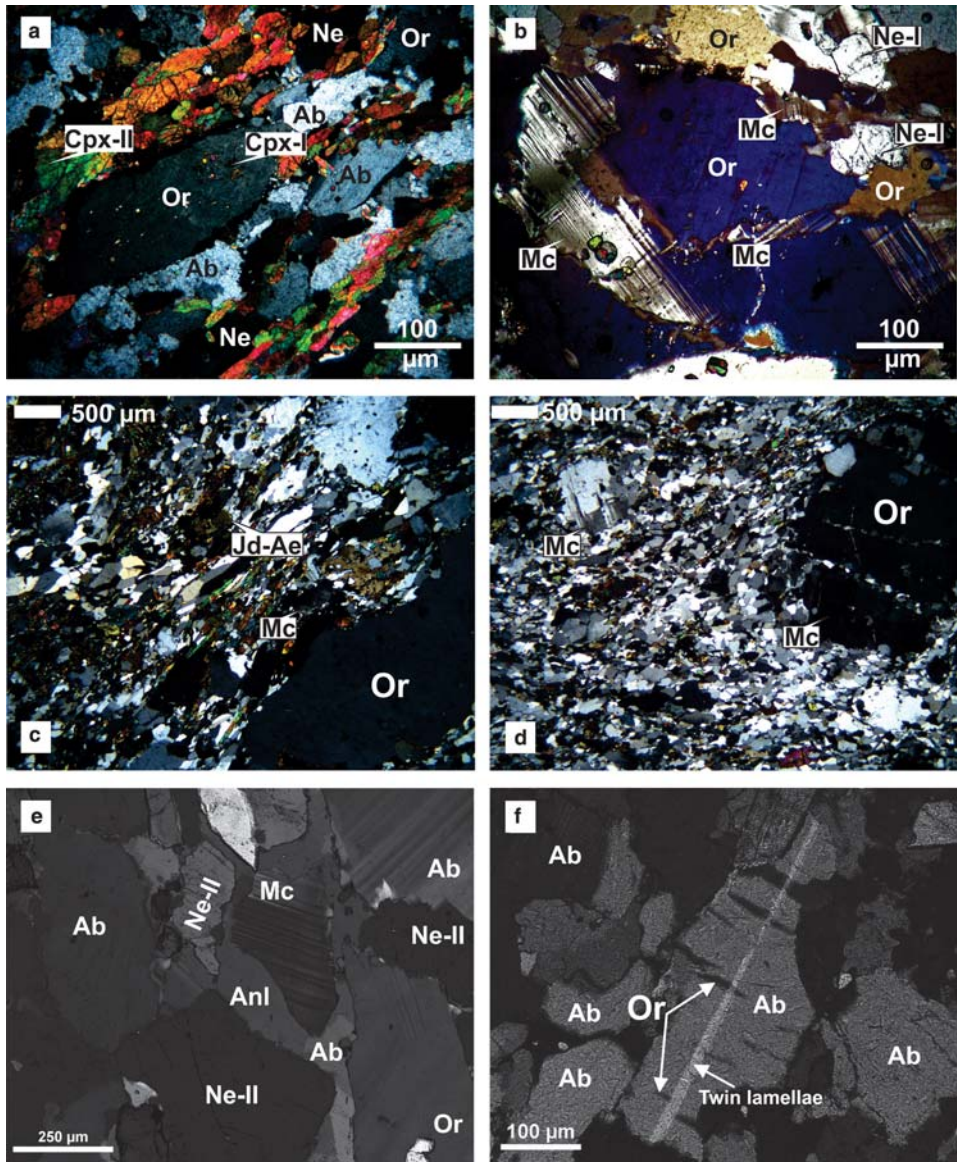

FIG. 2. Characteristic textures observed in Sushina (*a*,*b*,*e*,*f*) and Norra Kärr (*c*,*d*) agpaitic syenites. All images are in cross-polarized light. (*a*) Gneissic textures defined by alternating layers of felsic (orthoclase: Or, albite: Ab, nepheline: Ne-II) and mafic minerals (clinopyroxene: Cpx-II). Note at the centre a macrocryst of orthoclase containing numerous inclusions of early formed clinopyroxene (Cpx-I). (*b*) Microcline (Mc) formation (microclinization) along the grain boundary of a macrocryst of orthoclase (Or) suggestive of post-crystallization low temperature re-equilibration. (*c*) Incipient development of gneissosity defined by the aegirine–jadeite (Ae–Jd) and felsic minerals in catapleiite-syenite (grennaite) of the Norra Kärr complex. Note in common with Sushina the presence of large macrocrysts of orthoclase (Or). (*d*) Cataclastic texture in the catapleiite-syenite from the Nora Kärr complex and microclinization along the grain boundary of an orthoclase macrocryst. (*e*) Macrocrysts of albite (Ab), orthoclase (or) and nepheline (Ne-II) defining an overall macrocrystal-to-hypidiomorphic texture in eudialyte-syenite. Note that incipient development of cross-hatched twining (microcline: Mc) in orthoclase and formation of analcime at the expense of nepheline (Ne-II) and albite are suggestive of low-temperature subsolidus alteration process. (*f*) Antiperthite with relict twin lamellae of the host albite.

https://doi.org/10.1180/minmag.2016.080.057 Published online by Cambridge University Press

TABLE 1. Representative compositions of the feldspar group of minerals.

	Albite									Orthoclase		
	1	2	3	4	5	6	7	8	9	10	11	12
SiO_2	68.03	67.54	67.73	68.31	67.92	66.31	67.74	67.71	67.07	64.07	63.79	63.74
Al_2O_3	19.42	19.65	19.56	19.64	19.65	19.15	19.55	19.57	19.39	18.58	18.24	18.38
FeO	0.02	0.05	0.05	0.02	0.05	0.04	0.06	0.03	0.15	0.03	0.02	0.04
CaO	0.02	0.01	0.01	0.01	0.17	0.01	0.02	0.01	0.18	0.00	0.00	0.00
Na_2O	12.08	11.84	12.00	12.24	12.07	11.59	11.93	12.04	11.60	0.49	0.35	0.31
K_2O	0.11	0.07	0.11	0.05	0.06	0.07	0.13	0.14	0.05	16.28	16.27	16.59
Total	99.69	99.16	99.45	100.27	99.93	97.17	99.43	99.52	98.44	99.45	98.66	99.06
Formula based on 8 oxygen atoms												
Si	2.99	2.98	2.98	2.98	2.98	2.98	2.98	2.98	2.98	2.98	2.99	2.98
Al	1.01	1.02	1.01	1.01	1.02	1.02	1.01	1.02	1.02	1.02	1.01	1.01
Fe	0.00	0.00	0.00	0.00	0.00	0.00	0.00	0.00	0.01	0.00	0.00	0.00
Ca	0.00	0.00	0.00	0.00	0.01	0.00	0.00	0.00	0.01	0.00	0.00	0.00
Na	1.03	1.01	1.02	1.04	1.03	1.01	1.02	1.03	1.00	0.04	0.03	0.03
K	0.01	0.00	0.01	0.00	0.00	0.00	0.01	0.01	0.00	0.97	0.97	0.99
Sum	5.03	5.02	5.03	5.03	5.03	5.02	5.02	5.03	5.01	5.01	5.01	5.02
mol.% end-members												
Ab	99	100	99	100	99	100	99	99	99	4	3	3
An	0	0	0	0	1	0	0	0	1	0	0	0
Or	1	0	1	0	0	0	1	1	0	96	97	97

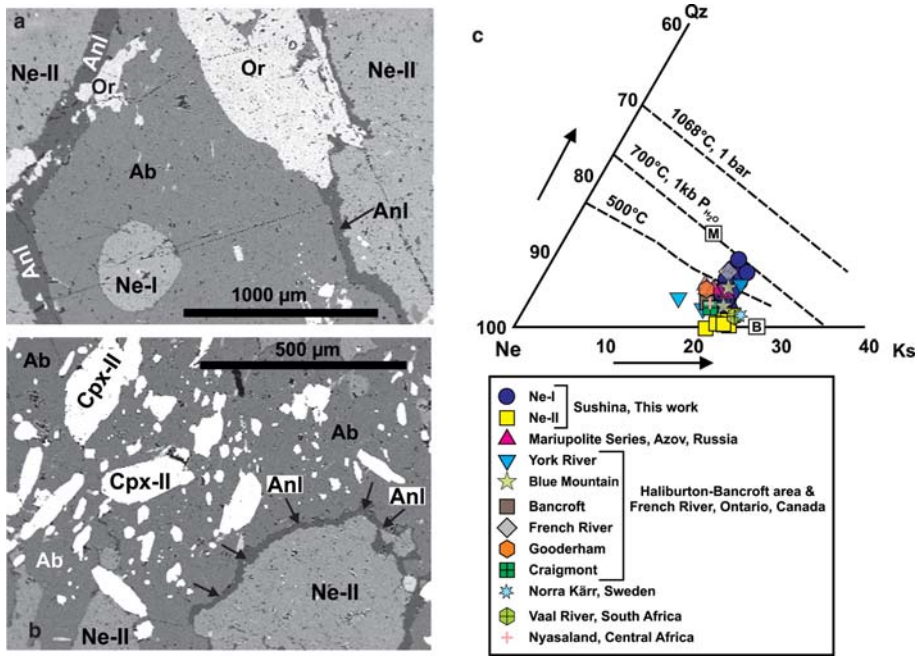

FIG. 3. Different textural modes of nepheline in Sushina agpaitic syenites. (*a*,*b*) are back-scattered electron (BSE) images. (*a*) Relict unaltered nepheline (Ne-I) present as inclusion within megacrystic albite. Note that the reaction texture involving nepheline (Ne-II) and albite (Ab) giving rise to analcime (Anl) are suggestive of low-temperature fluid activity in the agpaitic syenites (*b*) Inclusions of Ae–Jd rich Cpx-II within megacrystic albite. (*c*) Nepheline compositions of agpaitic syenites of Sushina plotted against nephelines from the metamorphosed agpaitic complexes (after Tilley, 1954).

within the megacrystic albite (Fig. 3*a*), whereas nepheline (Ne-II) occurs as veinlets replacing albite and in association with sodalite, analcime and natrolite and is commonly partially-altered to these phases. Reaction textures, mainly the formation of analcime involving nepheline (I and II) and albite in the presence of late-stage hydrothermal fluid are also evident (Fig. 3*a*,*b*). The least-altered nepheline (Ne-I) has the average composition $Ne_{72.6}Ks_{21.7}Qtz_{5.7}$ (wt.%) (Table 2, comp. 1–11) falling within the Morozewicz-Buerger convergence field of plutonic nepheline (Fig. 3*c*) suggesting an equilibration temperature of ~700°C. Altered and corroded nepheline (Ne-II) in immediate contact with natrolite and analcime approaches the stoichiometric Buerger composition ($Ne_{73}Ks_{27}$) (Fig. 3*c*) suggestive of significant cation exchange and re-equilibration with a sodium-rich deuteric or extraneous fluid. The close proximity to the ideal Morozewicz composition ($Ne_{75.0}Ks_{20.5}Qtz_{4.5}$) together with the presence of albite and microcline indicates that they are formed by either a plutonic or metasomatic/metamorphic environment (Tilley, 1954, 1957). Considering the reaction textures involving nepheline, i.e. alteration to sodalite and analcime (see below), it is evident that nepheline was formed under plutonic conditions and was later subjected to re-equilibration and/or metasomatism. Similar features are reported from the nepheline gneisses of Haliburton-Bancroft area, the Blue-Mountain nepheline syenite and Norra Kärr (Tilley, 1954, Duke and Edgar, 1977) and all are found to lie within the Morozewicz-Buerger field of convergence (Fig. 3*c*).

Clinopyroxene

Clinopyroxenes are the principal mafic minerals in the agpaitic gneisses and occur in two distinct textural modes. Early-formed euhedral clinopyroxenes (Cpx-I, ~200 μm) are either zoned or zonation-free and present as inclusions within large albite or orthoclase macrocrysts (Fig. 2*a*) and rarely within late-formed magnesio-arfvedsonite. The core of the zoned clinopyroxene is essentially diopsidic evolving to aegirine towards the rim (Table 3, comp. 1–7;

https://doi.org/10.1180/minmag.2016.080.057 Published online by Cambridge University Press

https://doi.org/10.1180/minmag.2016.080.057 Published online by Cambridge University Press

TABLE 2. Representative compositions of nepheline.

	Nepheline - I												Nepheline - II						
	1	2	3	4	5	6	7	8	9	10	11	12	13	14	15	16	17	18	19
SiO_2	41.57	41.62	41.92	41.92	41.71	41.30	41.58	41.35	41.26	41.25	42.98	42.80	40.63	41.55	41.32	42.99	42.72	40.64	41.18
Al_2O_3	34.42	34.65	34.39	34.03	34.17	34.64	34.55	34.82	34.43	34.64	34.37	33.75	34.95	33.18	34.14	31.84	32.62	34.73	34.20
FeO	0.18	0.17	0.20	0.19	0.18	0.18	0.15	0.15	0.16	0.12	0.20	0.15	0.07	0.10	0.07	0.16	0.11	0.11	0.17
CaO	0.00	0.00	0.00	0.04	0.02	0.02	0.00	0.00	0.02	0.00	0.01	0.03	0.00	0.00	0.02	0.02	0.02	0.00	0.00
Na_2O	15.37	15.40	15.55	15.41	15.34	15.27	15.48	15.24	15.07	14.89	16.14	15.47	15.59	16.26	16.06	17.38	16.93	15.58	15.74
K_2O	7.05	6.76	6.96	6.84	7.04	7.09	7.02	7.27	7.09	7.33	6.99	7.00	7.59	7.47	7.64	7.27	7.53	7.33	7.16
Total	98.59	98.60	99.02	98.42	98.46	98.50	98.78	98.84	98.03	98.23	100.69	99.20	98.83	98.56	99.25	99.66	99.94	98.39	98.45
Formula based 16 oxygen atoms																			
Si	4.07	4.06	4.08	4.10	4.09	4.05	4.06	4.04	4.06	4.05	4.12	4.15	3.99	4.09	4.04	4.20	4.16	4.00	4.05
Al	3.97	3.99	3.95	3.92	3.94	4.00	3.98	4.01	3.99	4.01	3.88	3.86	4.04	3.85	3.94	3.66	3.74	4.03	3.96
Fe	0.01	0.01	0.02	0.02	0.01	0.02	0.01	0.01	0.01	0.01	0.02	0.01	0.01	0.01	0.01	0.01	0.01	0.01	0.01
Ca	0.00	0.00	0.00	0.00	0.00	0.00	0.00	0.00	0.00	0.00	0.00	0.00	0.00	0.00	0.00	0.00	0.00	0.00	0.00
Na	2.92	2.92	2.93	2.92	2.91	2.90	2.93	2.89	2.87	2.83	3.00	2.91	2.97	3.11	3.05	3.29	3.19	2.97	3.00
K	0.88	0.84	0.86	0.85	0.88	0.89	0.87	0.91	0.89	0.92	0.85	0.87	0.95	0.94	0.95	0.91	0.93	0.92	0.90
mol.% end-members																			
Ne	72	72	72	71	71	72	72	71	71	70	73	70	74	76	75	78	77	74	74
Ks	22	21	21	21	22	22	22	22	22	23	21	21	24	23	24	22	22	23	22
Qtz	7	8	7	8	7	6	6	6	7	7	6	9	2	1	1	0	1	3	4

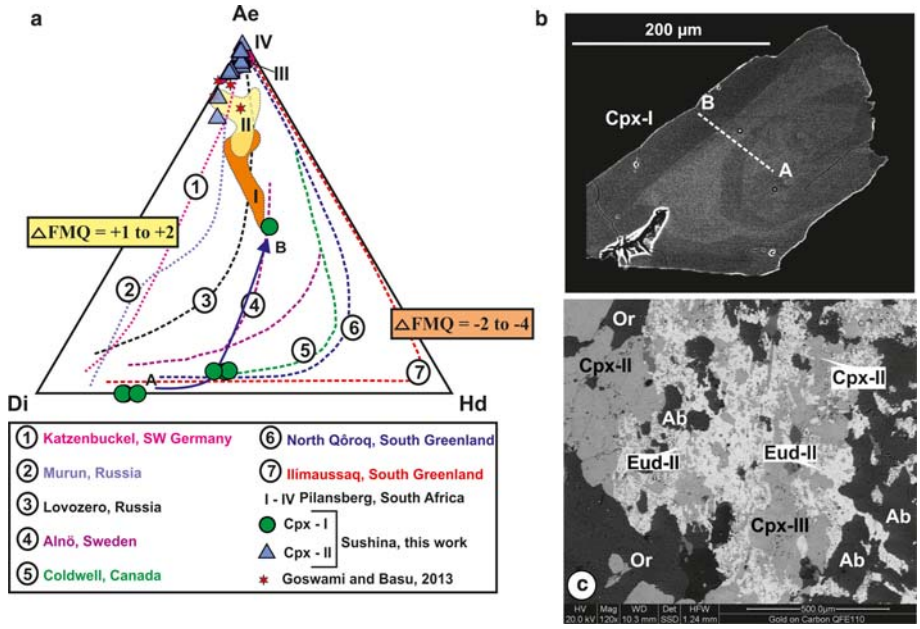

FIG. 4. Clinopyroxene evolution trends in the diopside (Di)-hedenbergite (Hd)-aegirine (Ae) ternary system (*a*) and their different textural modes of occurrence (BSE images *b*, *c*). Pyroxene evolution trend for other alkaline complexes are shown for comparison (after Marks *et al.* 2008 and references therein; Mitchell and Liferovich, 2006). (*a*) Early generations of zoned clinopyroxenes (Cpx-I in Fig. *b*) (green circles, blue line) are characterized by a diopsidic core and aegirine-rich rim. In contrast, clinopyroxenes with a significant aegirine–jadeite component (Cpx-II) are the dominant pyroxene present in the eudialyte-nepheline syenite (mint blue triangles). (*b*) Discrete grain of a rare zoned clinopyroxene (Cpx-I) with diopsidic core. (*c*) Post-magmatic eudialyte (Eud-II) showing a mesh-like texture engulfing and corroding clinopyroxene (Cpx-II). Remnant patches of orthoclase (Or) and albite (Ab) grains are preserved within such complex assemblages of Eud-II and Cpx-II.

Fig. 4*a*,*b*). Compositionally, Cpx-I are alumina-poor and the least-evolved in terms of their Na, Mg, Fe and Ca contents. Subhedral-to-anhedral elongated clinopyroxenes which define an incipient gneissosity (Cpx-II, Fig. 2*a*) are the dominant pyroxene in the agpaitic gneisses. However, anhedral and highly-corroded clinopyroxenes (Cpx-II) are also present in association with eudialyte and related alteration products, mainly pectolite and serandite (Fig. 4*c*). Compositionally, Cpx-II are poorer in CaO, TiO_2 but richer in Al_2O_3 (up to 4.26 wt.% Al_2O_3) compared to Cpx-I. These are essentially aegirine (up to 87 mol.%) with a significant jadeite component (up to 18 mol.%) (Table 3). However, some Cpx-II are enriched in diopside, hedenbergite and Ti-aegirine components (Table 3, comp. 23). The Zr contents of the pyroxenes are in general low, but can reach up to 3 wt.% ZrO_2 for some Cpx-II indicating a probable presence of zirconian aegirine component.

Figure 4*a* shows that Cpx-I is least evolved in terms of Fe, Mg, Ca and Na contents compared to Cpx-II and grades from primary magmatic diopside ($Di_{79}Hd_{21}$) to late-formed aegirine (Ae_{100}). The compositional trend of the zoned Cpx-I is comparable to the primary magmatic trend of Alnö pyroxenes (Vuorinen *et al.*, 2005) whereas that of the Cpx-II is similar to the hydrothermal pyroxenes of the Pilansberg complex (Mitchell and Liferovich, 2006) (Fig. 4*a*).

Metamorphosed agpaitic complexes such as Red Wine (Canada) and Norra Kärr (Sweden), are characterized generally by the presence of aegirine-jadeite similar to Cpx-II (Adamson, 1944; Curtis and Gittins, 1979). Such, Al, Fe^{3+} rich pyroxenes with significant aegirine and jadeite component are also reported from the Ilímaussaq clinopyroxene-lujavrite (Greenland) (Type 1 and 3 clinopyroxene of Markl *et al.*, 2001). In the Di–Hd–Ae ternary system it is difficult to distinguish between primary magmatic and aegirine-jadeite pyroxene as the

https://doi.org/10.1180/minmag.2016.080.057 Published online by Cambridge University Press

TABLE 3. Representative compositions of clinopyroxene.

	Clinopyroxene-I							Clinopyroxene-II		
	1	2	3	4	5	6	7	8	9	10
SiO_2	50.34	50.71	50.44	50.32	49.87	49.44	50.28	52.59	54.00	54.07
TiO_2	0.13	0.56	0.12	0.48	0.42	0.51	0.67	0.13	0.13	0.18
Al_2O_3	1.12	0.69	0.89	0.73	1.25	1.03	2.62	2.75	2.41	2.68
Cr_2O_3	0.00	0.00	0.00	0.00	0.00	0.00	0.01	0.00	0.01	0.00
Fe_2O_3	0.00	3.11	0.00	4.21	4.75	0.00	12.93	29.56	28.36	27.70
FeO	6.83	11.94	6.86	13.00	12.41	8.42	8.15	0.04	0.01	0.03
MnO	0.51	0.67	0.46	0.21	0.14	0.14	0.14	0.57	0.48	0.65
MgO	15.12	8.52	15.51	8.62	9.57	14.80	2.89	0.53	0.50	0.63
ZrO_2	0.00	0.12	0.10	0.02	0.19	0.10	0.01	0.15	0.19	0.20
CaO	25.32	23.18	24.72	22.12	21.09	25.28	16.63	1.01	0.86	1.09
Na_2O	0.61	0.78	0.89	0.79	0.71	0.54	5.59	12.98	13.44	13.31
K_2O	0.01	0.03	0.01	0.01	0.06	0.00	0.02	0.01	0.00	0.01
Sum	99.99	100.31	100.00	100.52	100.47	100.26	99.94	100.33	100.39	100.54
Formula based on 4 cations and 6 oxygen atoms										
Si	1.85	1.95	1.85	1.94	1.92	1.82	1.94	1.99	2.03	2.03
Al	0.05	0.03	0.04	0.03	0.06	0.05	0.12	0.12	0.11	0.12
Ti	0.00	0.02	0.00	0.01	0.01	0.01	0.02	0.00	0.00	0.01
Cr	0.00	0.00	0.00	0.00	0.00	0.00	0.00	0.00	0.00	0.00
Fe^{3+}	0.00	0.09	0.00	0.12	0.14	0.00	0.38	0.84	0.80	0.78
Mg	0.83	0.49	0.85	0.50	0.55	0.81	0.17	0.03	0.03	0.04
Fe^{2+}	0.21	0.38	0.21	0.42	0.40	0.26	0.26	0.00	0.00	0.00
Mn	0.02	0.02	0.01	0.01	0.01	0.00	0.01	0.02	0.02	0.02
Zr	0.00	0.00	0.00	0.00	0.00	0.00	0.00	0.00	0.00	0.00
Ca	1.00	0.96	0.97	0.91	0.87	1.00	0.69	0.04	0.04	0.04
Na	0.04	0.06	0.06	0.06	0.05	0.04	0.42	0.95	0.98	0.97
K	0.00	0.00	0.00	0.00	0.00	0.00	0.00	0.00	0.00	0.00
mol.% end-members										
Aeg	0	6	0	6	5	0	42	84	84	81
Jd	0	0	0	0	0	0	5	11	11	12
Ti-Aeg	1	0	1	0	0	3	0	0	2	2
Fe-Ts	0	2	0	3	4	0	0	0	0	0
Ti-Ts	0	2	0	1	2	0	2	1	0	0
Ca-Ts	0	0	0	0	1	0	2	0	0	0
Di	76	50	75	47	46	71	19	2	2	3
Hd	21	41	20	40	34	23	30	1	1	2
En	2	0	4	1	4	2	0	0	0	0
Fs	1	0	1	1	3	1	0	0	0	0

(continued on next page)

jadeite component cannot be incorporated in such a diagram. The $^{VI}Al/(^{VI}Al + Fe^{3+}) - Na/(Na + Ca)$ diagram (Curtis and Gittins, 1979) might be useful to distinguish the pyroxene types (Fig. 5). It is interesting to note that the Cpx-II ($Ae_{88}Jd_{10}$) of the Sushina agpaites shows remarkable similarities with the clinopyroxenes of (eudialyte-catapleiite nepheline syenite) grennaite ($Ae_{81}Jd_{18}$) and (arfvedsonite nepheline syenite) lakarpite ($Ae_{78}Jd_{11}$) of the Norra Kärr and aegirine lujavrite ($Ae_{91}Jd_6$) of the Ilímaussaq complexes, respectively being enriched in aegirine compared to jadeite (Fig. 5*a*,*c*). Zoned clinopyroxenes found in the grennaite shows an overall jadeite enrichment from core to rim ($Ae_{86}Jd_{12} \rightarrow Ae_{65}Jd_{34}$; this work) (Fig. 5*a*). In contrast, Red Wine and Two Tom Lake clinopyroxenes are characterized by a jadeiitic core and aegirine rich rim ($Ae_{29}Jd_{68} \rightarrow Ae_{58}Jd_{36}$; this work) (Fig. 5*b*). It must be noted here the two of Sushina pyroxene compositions falling within the aegirine-augite field can be attributed to the presence of a hedenbergite component.

https://doi.org/10.1180/minmag.2016.080.057 Published online by Cambridge University Press

TABLE 3. (*contd.*)

	Clinopyroxene-II									
	11	12	13	14	15	16	17	18	19	20
SiO_2	52.61	52.95	53.92	53.62	52.49	53.39	53.51	52.55	53.18	52.52
TiO_2	0.24	0.19	0.20	0.11	0.09	0.15	0.20	0.09	0.05	0.24
Al_2O_3	4.07	4.26	2.81	3.49	2.72	3.23	3.03	4.12	4.16	2.92
Cr_2O_3	0.00	0.01	0.00	0.00	0.00	0.00	0.02	0.02	0.00	0.01
Fe_2O_3	27.88	27.08	27.57	27.39	30.60	27.68	27.55	27.30	29.16	29.29
FeO	0.01	0.03	0.04	0.04	0.01	0.03	0.01	0.04	0.02	0.04
MnO	0.57	0.71	0.59	0.51	0.20	0.90	1.01	0.82	0.10	0.24
MgO	0.53	0.60	0.63	0.56	0.35	0.63	0.61	0.54	0.09	0.37
ZrO_2	0.00	0.18	0.20	0.23	0.00	0.18	0.22	0.22	0.01	0.08
CaO	0.91	1.10	1.04	0.92	0.66	1.22	1.27	1.06	0.11	0.72
Na_2O	13.02	13.01	13.29	13.27	13.19	13.02	13.05	12.90	13.62	13.18
K_2O	0.01	0.01	0.01	0.03	0.00	0.01	0.03	0.00	0.02	0.03
Sum	99.85	100.12	100.31	100.16	100.31	100.45	100.51	99.66	100.54	99.65
Formula based on 4 cations and 6 oxygen atoms										
Si	1.98	1.99	2.02	2.01	1.99	2.00	2.01	1.99	1.99	1.99
Al	0.18	0.19	0.12	0.15	0.12	0.14	0.13	0.18	0.18	0.13
Ti	0.01	0.01	0.01	0.00	0.00	0.00	0.01	0.00	0.00	0.01
Cr	0.00	0.00	0.00	0.00	0.00	0.00	0.00	0.00	0.00	0.00
Fe^{3+}	0.79	0.77	0.78	0.77	0.87	0.78	0.78	0.78	0.82	0.84
Mg	0.03	0.03	0.04	0.03	0.02	0.04	0.03	0.03	0.01	0.02
Fe^{2+}	0.00	0.00	0.00	0.00	0.00	0.00	0.00	0.00	0.00	0.00
Mn	0.02	0.02	0.02	0.02	0.01	0.03	0.03	0.03	0.00	0.01
Zr	0.00	0.00	0.00	0.00	0.00	0.00	0.00	0.00	0.00	0.00
Ca	0.04	0.04	0.04	0.04	0.03	0.05	0.05	0.04	0.00	0.03
Na	0.95	0.95	0.97	0.97	0.97	0.95	0.95	0.95	0.99	0.97
K	0.00	0.00	0.00	0.00	0.00	0.00	0.00	0.00	0.00	0.00
mol.% end-members										
Aeg	79	77	81	79	87	79	79	78	82	84
Jd	16	18	13	16	10	14	14	17	17	12
Ti-Aeg	0	1	2	1	0	2	2	0	0	1
Fe-Ts	0	0	0	0	0	0	0	0	0	0
Ti-Ts	1	1	0	0	0	0	0	1	0	0
Ca-Ts	0	0	0	0	1	0	0	0	0	0
Di	2	2	3	2	1	3	3	2	0	2
Hd	1	2	2	1	0	2	3	2	0	1
En	1	0	0	0	0	0	0	1	0	0
Fs	0	0	0	0	0	0	0	1	0	0

(continued on next page)

Late-magmatic eudialyte

Eudialyte is the dominant typomorphic mineral present in these agpaitic gneisses. Two types of eudialyte (late magmatic and post-magmatic/hydrothermal) are found, and are distinguished by the intensity of the pink pleochroism and their composition (Chakrabarty *et al.*, 2012; Mitchell and Chakrabarty, 2012) (Fig. 6). Late-magmatic eudialytes are present as remnant macrocrysts (Figs 6*a*,*b* and 7) whereas the post-magmatic eudialytes typically exhibit a mesh-like texture as reported by Mahato *et al.* (2013) (Figs 4*c* and 6*c*,*d*). Late magmatic eudialytes are characterized by pale pink pleochroism and are rich in Ca (>11.15 wt.% CaO) but poorer in Mn (6.64–8.34 wt.% MnO), *REE* and Sr (0.64–1.22 wt.% SrO) compared to the strongly-pleochroic post-magmatic eudialyte (Table 4). In

https://doi.org/10.1180/minmag.2016.080.057 Published online by Cambridge University Press

TABLE 3. (*contd*.)

	Clinopyroxene-II										
	21	22	23	24	25	26	27	28	29	30	31
SiO_2	53.34	53.09	50.17	53.64	53.06	53.28	53.18	52.43	52.03	52.20	52.06
TiO_2	0.22	0.34	0.19	0.26	0.43	0.33	0.46	0.45	0.14	0.22	0.11
Al_2O_3	4.08	3.75	2.60	2.66	2.44	2.44	2.52	2.47	2.18	2.46	1.95
Cr_2O_3	0.00	0.02	0.00	0.00	0.00	0.00	0.00	0.00	0.00	0.00	0.00
Fe_2O_3	26.98	27.18	5.35	25.60	27.35	28.47	27.93	26.89	29.18	24.04	28.13
FeO	0.05	0.02	16.16	0.01	0.02	0.09	0.03	0.01	0.00	0.03	0.07
MnO	0.63	0.77	0.67	0.43	0.28	0.29	0.13	0.26	0.21	1.08	0.16
MgO	0.47	0.58	2.55	2.18	2.18	1.17	0.44	1.14	0.25	2.50	1.15
ZrO_2	0.15	0.29	3.85	0.12	0.11	0.02	0.02	0.01	0.03	0.00	0.00
CaO	0.93	1.08	14.00	3.21	1.74	1.90	0.42	1.84	0.49	6.02	2.08
Na_2O	13.23	13.10	4.92	12.07	12.39	12.73	13.48	12.59	13.17	10.63	12.38
K_2O	0.01	0.01	0.09	0.01	0.01	0.03	0.01	0.02	0.00	0.01	0.00
Sum	100.09	100.24	100.55	100.20	100.01	100.74	98.62	98.11	97.68	99.19	98.09
Formula based on 4 cations and 6 oxygen atoms											
Si	2.00	1.99	1.97	2.01	2.00	2.00	2.03	2.01	2.02	1.99	2.00
Al	0.18	0.17	0.12	0.12	0.11	0.11	0.11	0.11	0.10	0.11	0.18
Ti	0.01	0.01	0.01	0.01	0.01	0.01	0.01	0.01	0.00	0.01	0.01
Cr	0.00	0.00	0.00	0.00	0.00	0.00	0.00	0.00	0.00	0.00	0.00
Fe^{3+}	0.76	0.77	0.16	0.72	0.78	0.80	0.80	0.78	0.85	0.69	0.76
Mg	0.03	0.03	0.15	0.12	0.12	0.07	0.03	0.07	0.01	0.14	0.03
Fe^{2+}	0.00	0.00	0.53	0.00	0.00	0.00	0.00	0.00	0.00	0.00	0.00
Mn	0.02	0.03	0.02	0.01	0.01	0.01	0.00	0.01	0.01	0.04	0.02
Zr	0.00	0.01	0.07	0.00	0.00	0.00	0.00	0.00	0.00	0.00	0.00
Ca	0.04	0.04	0.59	0.13	0.07	0.08	0.02	0.08	0.02	0.25	0.04
Na	0.96	0.95	0.38	0.88	0.90	0.93	1.00	0.94	0.99	0.78	0.96
K	0.00	0.00	0.01	0.00	0.00	0.00	0.00	0.00	0.00	0.00	0.00
mol.% end-members											
Aeg	76	77	16	73	77	81	84	80	87	71	83
Jd	18	16	9	12	10	11	12	11	10	10	9
Ti-Aeg	2	3	13	2	2	2	3	3	1	0	1
Fe-Ts	0	0	0	0	0	0	0	0	0	0	0
Ti-Ts	0	0	1	0	0	0	0	0	0	1	0
Ca-Ts	0	0	0	0	0	0	0	0	0	0	0
Di	2	2	12	11	6	6	1	5	1	15	6
Hd	2	2	45	1	0	1	0	1	1	4	1
En	0	0	1	0	2	0	0	0	0	0	0
Fs	0	0	3	0	0	0	0	0	0	0	0

Aeg: Aegirine [$NaFe^{3+}Si_2O_6$], Jd: Jadeite [$NaAlSi_2O_6$], Ti-Aeg: Ti-Aegirine [$Na(Ti_{0.5}Fe_{0.5})Si_2O_6$], Fe-Ts: Fe-Tschermak [$CaFe(FeSiO_6)$], Ti-Ts: Ti-Tschermak [$CaTiAl_2O_6$], Ca-Ts: Ca-Tschermak [$CaAl(AlSiO_6)$], Di: Diopside [$CaMgSi_2O_6$], Hd: Hedenbergite [$CaFe^{2+}Si_2O_6$], En: Enstatite [$Mg_2Si_2O_6$], Fs: Ferrosilite [$Fe_2Si_2O_6$].

general both the variants are enriched in Mn compared to other reported occurrences of eudialyte from the agpaitic nepheline syenites (Schilling *et al.*, 2011*a*; Aksenov *et al.*, 2014) and comparable with those of the late- to post-magmatic eudialyte of the Pilansberg lujavrite and Norra Kärr metamorphosed agpaites (Mitchell and Liferovich, 2006; Sjöqvist *et al.*, 2013). However, both types are partially- or completely-altered by the subsolidus deuteric/hydrothermal process during the post-magmatic stage.

Other minerals

Long needle-like prismatic crystals of rinkite (5–10 μm) are present as inclusions within late

https://doi.org/10.1180/minmag.2016.080.057 Published online by Cambridge University Press

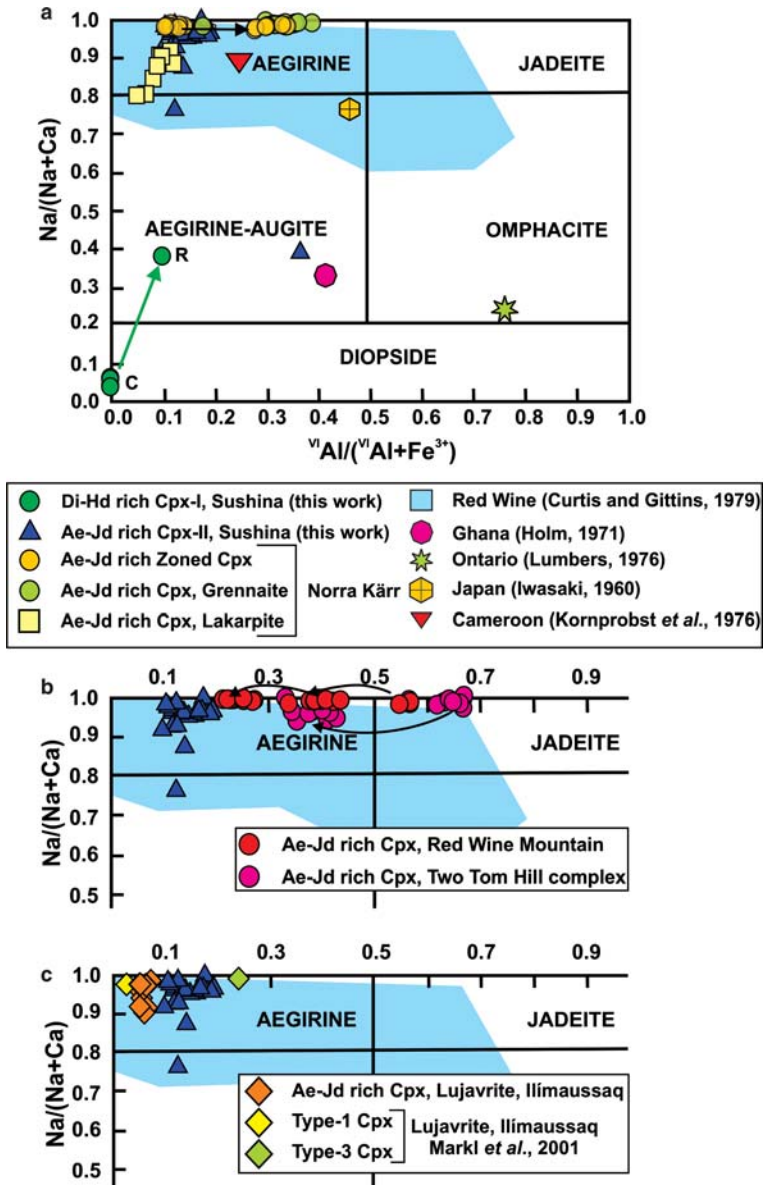

FIG. 5. (*a*) The composition of clinopyroxenes plotted in $^{VI}Al/(^{VI}Al+Fe^{3+})$ – Na/(Na+Ca) diagram (after Curtis and Gittins, 1979) showing an enrichment in aegirine content of Cpx-I from core to rim. In contrast Cpx-II plot within the aegirine field similar to aegirine–jadeite (Ae–Jd) clinopyroxene of lakarpite of the metamorphosed Norra Kärr alkaline complex. Note jadeite enrichment from core to rim for zoned Ae–Jd clinopyroxene from grennaite, Norra Kärr. (*b*) Zoned Ae–Jd rich clinopyroxene from metamorphosed Red Wine Mountain and Two Tom Lake Complex showing a reverse trend of jadeiitic core to aegirine rich rim. (*c*) Jadeite rich clinopyroxene from Ilímaussaq alkaline complex showing remarkable similarity with the Cpx-II of the Sushina. The arrow indicates core–rim compositional variation in all the diagrams.

magmatic eudialyte (Fig. 7) and rarely within albite. Such textural features indicate that rinkite predates these phases and is thus considered as a relict primary phase (Chakrabarty *et al.*, 2013). Rinkite in these gneisses is rich in Nd and F and compositionally similar to those reported by

https://doi.org/10.1180/minmag.2016.080.057 Published online by Cambridge University Press

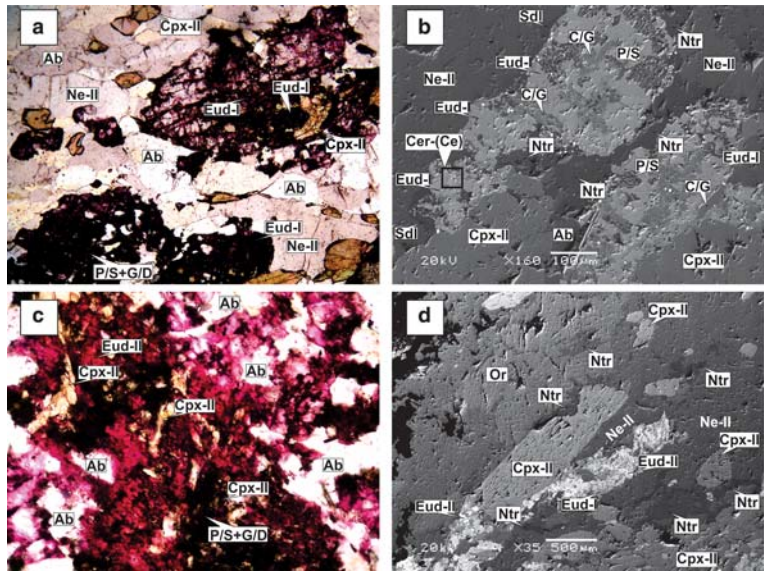

FIG. 6. (*a*) Eudialyte macrocryst (Eud-I) associated with nepheline (Ne-II), albite (Ab) and clinopyroxene (Cpx-II). Anhedral clinopyroxene (Cpx-II) is associated with eudialyte. Plane-polarized light image. (*b*) BSE image illustrating eudialyte decomposition assemblage of pectolite–serandite (P/S), catapleiite/gaidonnyaite (C/G) and cerianite-(Ce) [Cer-(Ce)]. Nepheline (Ne-II) adjacent to eudialyte is marginally altered to sodalite (Sdl). Elongated anhedral natrolite grain associated with nepheline (Ne-II) is also present. (*c*) Post-magmatic eudialyte (Eud-II) occurring with a mesh-like texture in association with extensively-corroded clinopyroxene (Cpx-II) and albite (Ab). Note that the difference in pleochroism between late- and post-magmatic eudialyte in shades of pink. Plane-polarized light image. (*d*) BSE image showing the pervasive nature of natrolite (Ntr) cross cutting all precursor minerals illustrating its late-stage formation in the overall paragenesis compared to major silicate phases such as orthoclase (Or), albite (Ab), clinopyroxenes and eudialyte. Note that the post-magmatic eudialyte (Eud-II) overgrow the late-magmatic eudialyte (Eud-I).

Chakrabarty *et al.* (2013). In addition to rinkite, various Nb- rich minerals such as nacareniobsite-(Ce), marianoite and wöhlerite are also found in the agpaitic gneisses. Rare occurrences of arfvedsonitic amphiboles (<1 modal%) are also found in some places in the gneisses (Fig. 8). These alkali amphiboles are characterized by an elevated content of Mn (>7 wt.% MnO, Table 5), and classified as manganoan magnesio-arfvedsonite. They contain inclusions of Cpx-I and are marginally-altered to biotite. With respect to the Mn enrichment of both the amphibole- and eudialyte-group minerals, we consider these minerals were formed concurrently during the late-magmatic stage.

The primary magmatic assemblage discussed above is quite similar to those observed at the Norra Kärr and Red Wine complexes, where more-deformed, metasomatically-altered rocks are volumetrically dominant, while the least-altered rocks with prominent igneous textures and mineral assemblages are present as remnant patches within envelopes of deformed rocks.

Secondary minerals formed by hydrothermal processes

Post-magmatic eudialyte

As noted above, strongly-pleochroic eudialytes are found to overgrow pre-existing late-magmatic eudialyte (Fig. 6*d*). These eudialytes are generally anhedral in habit and typically show a mesh-like texture engulfing the pyroxenes (Cpx-II) and albite (Chakrabarty, 2009; Mahato *et al.*, 2013) (Fig. 4*d*). A similar textural feature associated with eudialyte is also reported from the lujavrite of the Pilansberg complex by Olivo and Williams-Jones (1999). Compositionally, post-magmatic eudialytes are characterized by elevated contents of Mn (>8 wt.% MnO), *REE* (>2 wt.% REE_2O_3) and SrO (>1.7 wt.% SrO) (Table 6, comp. 1–3).

Analcime

Analcime occurs as turbid anhedral grains and reaction rims at the contact between nepheline and

https://doi.org/10.1180/minmag.2016.080.057 Published online by Cambridge University Press

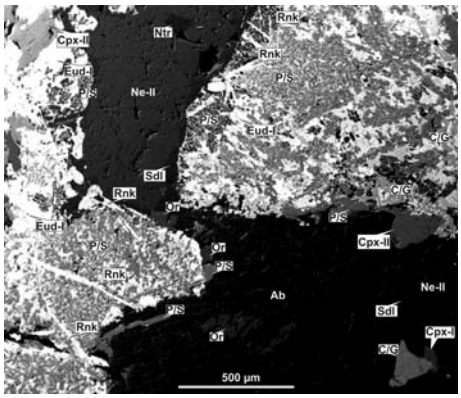

FIG. 7. BSE image illustrating decomposition assemblages pseudomorphing late-magmatic eudialyte macrocrysts (Eud-I). Elongated needle shaped rinkite (Rnk) crystals are present as inclusions within Eud-I. The decomposition assemblage is mainly represented by pectolite–serandite (P/S) and catapleiite/gaidonnyaite (C/G). Extensively-corroded clinopyroxenes (Cpx-II) are also present within the eudialyte decomposition assemblage. Chlorine released by the decomposing eudialyte reacted with adjacent nepheline (Ne-II) to form sodalite (Sdl). In some places alteration of nepheline (Ne-II) to natrolite (Ntr) also occurs. Note the catapleiite/gaidonnyaite present within the eudialyte decomposition assemblage and also as discrete grains.

albite grains (Fig. 3*a*,*b*). The composition of the analcime (Table 7, comp. 1–5) approaches the ideal stoichiometric composition of $NaAlSi_2O_6 \cdot H_2O$. Similar analcimes have been reported from the Pilansberg (Mitchell and Liferovich, 2006) and Mont Saint Hilaire complexes (Schilling *et al.*, 2011*b*).

Natrolite

Natrolite is the latest aluminosilicate to form. It corrodes and replaces all precursor feldspars, nepheline, aegirine and amphibole (Figs 6*b* and 7). In places the replacement is so extensive that eudialyte and its decomposition assemblages, represented by pectolite–serandite solid solution and hilairite, are also replaced by the late-forming natrolite (Fig. 6*d*). Typically, all natrolite as seen in BSE images (Fig. 6) appears to be anhedral in habit and has crystallized along fractures in the replaced minerals. Compositionally, natrolite is characterized by relatively low analytical totals in the range of 88.52–89.99 wt.% with 3.00–3.04 apfu Si; 1.81–1.89 apfu Na and 2.01–2.05 apfu Al (Table 7, comp. 6–14), and quite similar to the reported occurrences of late-stage natrolite from the Pilansberg (Mitchell and Liferovich, 2006) and Mont Saint Hilaire (Schilling *et al.*, 2011*b*) peralkaline complexes.

Sodalite

Sodalite is found typically in association with the decomposition assemblage formed after eudialyte, particularly where decomposing eudialyte released Cl^- ions which reacted with the adjacent nepheline to form sodalite (Fig. 7). Compositionally, sodalities are rich in Cl^- (>7 wt.%, Table 8) and approach the ideal formula of $Na_8Al_6Si_6O_{24}Cl_2$ with the sum of the tetrahedrally-coordinated Si and Al cations being close to the ideal value of 12. The Cl content of the sodalite is quite high (close to ideal value of 2 apfu, Table 8) compared to other reported occurrences, as in the Pilansberg (Mitchell and Liferovich, 2006) and Mont Saint Hilaire (Schilling *et al.*, 2011*b*) complexes, reflecting the dominance of the NaCl component in the fluid responsible for the transformation of nepheline to sodalite.

Biotite

Minerals of the mica group are rare in the agpaitic gneiss and found mainly replacing clinopyroxene (Cpx-II) or manganoan magnesio-arfvedsonite (Fig. 8). Compositionally, they are characterized by relatively higher concentrations of Mn (>10.9 wt.% MnO), Zn (1.28–1.46 wt.% ZnO) with low Fe/(Fe + Mg) ratios ranging between 0.37 and 0.47 (Table 9). According to the classification of Tischendorf *et al.* (2007) these micas can be classified as trioctahedral micas and are representative of the phlogopite – annite series with $^{VI}Al > 0.5$ and $Mg \times Li > 0.3$. The presence of Zn in these micas indicates an additional minor hendricksite component together with phlogopite and annite. However, for simplicity we prefer the root name biotite (hereafter) which is commonly used for trioctahedral micas between or close to the annite–phlogopite and siderophyllite–eastonite joins (Reider *et al.*, 1998). Compositionally these biotites are similar to the recrystallized primary biotites of Nachit *et al.* (2005). However, textural features, particularly replacement of pyroxene and amphibole by biotite, clearly indicate that these biotites are secondary and formed at a late stage relative to pyroxene and amphibole.

Other minerals

Eudialyte found in these gneisses is typically decomposed to a pectolite–serandite

https://doi.org/10.1180/minmag.2016.080.057 Published online by Cambridge University Press

TABLE 4. Representative compositions of late magmatic eudialyte.

	1	2	3	4	5	6	7	8	9	10
Nb_2O_5	3.26	3.02	3.14	4.03	3.73	3.67	3.44	0.81	3.60	3.83
SiO_2	46.82	46.84	46.29	46.45	45.99	46.02	45.97	51.19	45.68	46.95
TiO_2	0.10	0.11	0.09	0.03	0.00	0.03	0.05	0.03	0.00	0.03
ZrO_2	10.33	10.48	10.35	9.50	11.81	14.09	11.76	8.28	10.76	11.08
HfO_2	0.12	0.12	0.12	0.12	0.11	0.25	0.20	0.11	0.19	0.15
Al_2O_3	0.00	0.00	0.00	0.16	0.00	0.00	0.00	1.36	0.02	0.00
Y_2O_3	n.a.	n.a.	n.a.	n.a.	n.a.	n.a.	n.a.	n.a.	n.a.	n.a.
La_2O_3	0.21	0.25	0.30	0.28	0.67	0.47	0.56	0.15	0.58	0.38
Ce_2O_3	0.63	0.62	0.70	1.00	1.65	1.27	1.38	0.27	1.48	1.22
Nd_2O_3	0.19	0.23	0.24	0.35	0.59	0.47	0.56	0.11	0.50	0.44
Pr_2O_3	0.07	0.07	0.01	0.08	0.15	0.01	0.13	0.00	0.11	0.13
FeO	0.07	0.04	0.04	0.04	0.06	0.03	0.08	0.15	0.09	0.11
MnO	7.42	7.32	7.35	8.34	7.19	6.64	7.11	7.72	7.49	7.91
CaO	12.95	12.91	13.00	14.01	11.32	11.15	11.67	15.90	12.51	12.95
SrO	1.22	1.03	1.35	0.64	1.02	0.92	0.85	0.00	0.82	1.01
Na_2O	10.22	10.78	10.20	9.43	9.70	9.91	9.90	9.83	10.64	9.41
K_2O	0.51	0.50	0.53	0.41	0.46	0.46	0.48	0.11	0.59	0.58
F	0.33	0.01	0.22	0.25	0.16	0.06	0.01	0.62	0.00	0.14
Cl	0.59	0.68	0.69	0.46	0.73	0.58	0.67	0.11	0.49	0.61
Total	96.04	97.00	97.61	99.58	100.35	102.05	101.82	104.74	104.58	106.94
F≡O	0.14	0.00	0.09	0.11	0.07	0.03	0.00	0.26	0.00	0.06
Cl≡O	0.13	0.15	0.16	0.10	0.16	0.13	0.15	0.02	0.11	0.14
Total	94.78	94.84	94.37	95.37	95.13	95.91	94.67	96.46	95.49	96.75
Formula based on $\sum(Si + Zr + Ti + Nb + Al + Hf) = 29$ apfu										
Nb	0.80	0.74	0.78	0.99	0.91	0.88	0.85	0.18	0.90	0.93
Si	25.41	25.42	25.40	25.34	24.94	24.42	24.99	25.93	25.17	25.14
Ti	0.04	0.04	0.04	0.01	0.00	0.01	0.02	0.01	0.00	0.01
Zr	2.73	2.77	2.77	2.53	3.12	3.65	3.12	2.05	2.89	2.89
Hf	0.02	0.02	0.02	0.02	0.02	0.04	0.03	0.02	0.03	0.02
Al	0.00	0.00	0.00	0.10	0.00	0.00	0.00	0.81	0.02	0.00
Y	n.a.	n.a.	n.a.	n.a.	n.a.	n.a.	n.a.	n.a.	n.a.	n.a.
La	0.04	0.05	0.06	0.06	0.13	0.09	0.11	0.03	0.12	0.08
Ce	0.13	0.12	0.14	0.20	0.33	0.25	0.27	0.05	0.30	0.24
Nd	0.04	0.04	0.05	0.07	0.11	0.09	0.11	0.02	0.10	0.08

(continued)

TABLE 4. (*contd.*)

	1	2	3	4	5	6	7	8	9	10
Pr	0.01	0.01	0.00	0.02	0.03	0.00	0.03	0.00	0.02	0.03
Fe	0.03	0.02	0.02	0.02	0.03	0.01	0.04	0.06	0.04	0.05
Mn	3.41	3.36	3.41	3.85	3.30	2.98	3.27	3.31	3.50	3.59
Ca	7.53	7.51	7.64	8.19	6.58	6.34	6.80	8.63	7.38	7.43
Sr	0.38	0.32	0.43	0.20	0.32	0.28	0.27	0.00	0.26	0.31
Na	10.75	11.34	10.85	9.97	10.20	10.20	10.43	9.65	11.37	9.77
K	0.35	0.34	0.37	0.29	0.32	0.31	0.33	0.07	0.41	0.40
F	0.56	0.02	0.38	0.44	0.27	0.11	0.02	1.00	0.00	0.24
Cl	0.54	0.63	0.64	0.42	0.67	0.52	0.62	0.09	0.45	0.56

TABLE 5. Representative composition of manganoan magnesio-arfvedsonite.

	1	2	3
SiO_2	50.86	50.77	50.52
TiO_2	0.01	0.02	0.02
Al_2O_3	1.07	1.00	1.31
Cr_2O_3	0.00	0.00	0.00
Fe_2O_3	8.81	8.48	8.83
FeO	1.96	1.96	0.69
MnO	7.02	7.40	8.26
MgO	11.94	11.89	11.94
CaO	0.50	0.58	1.07
Na_2O	8.72	8.76	8.23
K_2O	1.45	1.44	1.47
H_2O*	1.94	1.94	1.94
Total	94.28	94.24	94.28
Formula based on 23 oxygen atoms			
Si	7.86	7.86	7.81
Al iv	0.14	0.14	0.19
∑T	8.00	8.00	8.00
Al vi	0.05	0.04	0.05
Ti	0.00	0.00	0.00
Cr	0.00	0.00	0.00
Fe^{3+}	1.02	0.99	1.03
Fe^{2+}	0.25	0.25	0.09
Mn	0.92	0.97	1.08
Mg	2.75	2.74	2.75
∑C	5.00	5.00	5.00
Ca	0.08	0.10	0.18
Na	1.92	1.90	1.82
∑B	2.00	2.00	2.00
Na	0.69	0.73	0.65
K	0.29	0.28	0.29
∑A	0.98	1.01	0.94
OH*	2.00	2.00	2.00

*OH is calculated after Mogessie *et al.* (2001).

[($NaCa_2Si_3O_8(OH)$–$NaMn_2^{2+}Si_3O_8(OH)$] assemblage (Table 6, comp. 4–6) together with diverse sodian-zirconosilicates such as catapleiite/gaidonnyaite ($Na_2ZrSi_3O_9{\cdot}2H_2O$) (Table 6, comp. 7–9) and hilairite ($Na_2ZrSi_3O_9.3H_2O$) (also see Mitchell and Chakrabarty, 2012). Other minerals found within the eudialyte decomposition assemblage include: cerianite-(Ce); pyrochlore; perraultite; ceriothorianite, together with rare wadeite and celsian (Mitchell and Chakrabarty, 2012; Chakrabarty *et al.*, 2013). Goswami and Basu (2013) reported the occurrence of cancrinite, piemontite and epidote from this variety of agpaitic gneiss, although we did not find any of these phases either as discrete grains or within the alteration

https://doi.org/10.1180/minmag.2016.080.057 Published online by Cambridge University Press

TABLE 6. Representative compositions of post-magmatic eudialyte, catapleiite/gaidonnayite and pectolite–serandite.

	Eudialyte (Eud)			Catapleiite/Gaidonnayite (C/G)			Pectolite-Serandite (P/S)		
	1	2	3	4	5	6	7	8	9
Nb_2O_5	3.67	3.22	2.64	0.00	0.00	0.00	0.24	0.23	0.11
SiO_2	46.43	46.65	47.34	47.50	47.48	47.78	52.24	51.99	52.30
TiO_2	0.16	0.16	0.10	0.00	0.03	0.01	0.00	0.02	0.02
ZrO_2	10.55	10.21	13.76	31.75	30.70	32.26	0.62	0.46	0.00
HfO_2	0.09	0.00	0.10	0.31	0.41	0.22	0.00	0.00	0.00
Al_2O_3	0.04	0.26	0.39	0.06	0.04	0.01	0.00	0.02	0.03
Y_2O_3	0.00	0.00	0.00	0.00	0.00	0.00	0.00	0.00	0.00
La_2O_3	1.21	1.20	0.86	0.00	0.10	0.03	0.08	0.04	0.00
Ce_2O_3	1.01	1.15	0.67	0.02	0.14	0.07	0.08	0.11	0.01
Nd_2O_3	0.53	0.52	0.57	0.07	0.00	0.01	0.08	0.02	0.04
FeO	0.22	0.07	0.06	0.88	0.01	0.05	0.05	0.06	0.10
MnO	8.84	8.93	7.05	0.07	0.75	0.00	19.08	20.16	19.78
CaO	8.81	8.85	7.76	0.82	1.82	0.58	16.60	16.43	17.44
SrO	1.95	2.02	1.77	0.00	0.00	0.00	0.00	0.00	0.00
Na_2O	10.92	12.67	9.61	12.57	11.14	12.60	9.79	9.77	9.42
K_2O	0.47	0.45	0.40	0.06	0.10	0.09	0.03	0.00	0.02
F	0.19	0.03	0.34	0.63	0.57	1.00	0.15	0.00	0.00
Cl	0.54	0.52	0.47	0.01	0.05	0.00	0.04	0.02	0.00
Total	95.62	96.90	93.90	94.76	93.36	94.71	99.06	99.33	99.26
F≡O	0.08	0.01	0.14	0.26	0.24	0.42	0.06	0.00	0.00
Cl≡O	0.12	0.12	0.11	0.00	0.01	0.00	0.01	0.00	0.00
Total	95.42	96.77	93.65	94.49	93.11	94.28	98.99	99.33	99.26
Formula based on $\sum$(Si + Zr + Ti + Nb + Al + Hf) = 29 apfu (Eud), 9 (C/G) and 8.5 (P/S) oxygen atoms									
Nb	0.90	0.79	0.62	0.00	0.00	0.00	0.01	0.01	0.00
Si	25.20	25.29	24.60	3.03	3.06	3.03	2.98	2.97	2.97
Ti	0.07	0.06	0.04	0.00	0.00	0.00	0.00	0.00	0.00
Zr	2.79	2.70	3.49	0.99	0.96	1.00	0.02	0.01	0.00
Hf	0.01	0.00	0.02	0.01	0.01	0.00	0.00	0.00	0.00
Al	0.02	0.16	0.24	0.01	0.00	0.00	0.00	0.00	0.00
Y	0.00	0.00	0.00	0.00	0.00	0.00	0.00	0.00	0.00
La	0.24	0.24	0.17	0.00	0.00	0.00	0.00	0.00	0.00
Ce	0.20	0.23	0.13	0.00	0.00	0.00	0.00	0.00	0.00
Nd	0.10	0.10	0.11	0.00	0.00	0.00	0.00	0.00	0.00
Fe	0.10	0.03	0.03	0.05	0.00	0.00	0.00	0.00	0.01
Mn	4.06	4.10	3.10	0.00	0.04	0.00	0.92	0.97	0.95
Ca	5.13	5.14	4.32	0.06	0.13	0.04	1.01	1.00	1.06
Sr	0.61	0.63	0.54	0.00	0.00	0.00	0.00	0.00	0.00
Na	11.50	13.31	9.69	1.55	1.39	1.55	1.08	1.08	1.04
K	0.33	0.31	0.27	0.01	0.01	0.01	0.00	0.00	0.00
F	0.32	0.05	0.57	0.13	0.12	0.20	0.03	0.00	0.00
Cl	0.50	0.48	0.41	0.00	0.01	0.00	0.00	0.00	0.00

assemblages associated with nepheline, albite or eudialyte. Sporadic occurrences of Mn-rich spessartine garnet were also noticed (Table 10) and have not been reported previously from these gneisses.

Discussion

Agpaitic nepheline syenites are essentially formed from an extremely-differentiated parent mafic

https://doi.org/10.1180/minmag.2016.080.057 Published online by Cambridge University Press

TABLE 7. Representative compositions of zeolite-group minerals.

	Analcime					Natrolite								
	1	2	3	4	5	6	7	8	9	10	11	12	13	14
SiO_2	53.54	53.52	54.32	53.56	53.92	47.41	47.40	47.44	47.49	47.50	47.14	47.05	47.21	47.19
Al_2O_3	23.14	23.23	23.00	23.30	23.80	27.10	27.51	27.11	26.81	27.21	27.07	26.93	26.59	26.95
FeO	0.01	0.02	0.04	0.01	0.01	0.04	0.02	0.02	0.03	0.01	0.00	0.00	0.04	0.02
MgO	0.00	0.00	0.00	0.00	0.00	0.00	0.00	0.00	0.00	0.00	0.00	0.00	0.00	0.00
CaO	0.00	0.01	0.08	0.04	0.01	0.06	0.04	0.04	0.03	0.11	0.09	0.05	0.02	0.01
Na_2O	13.88	13.59	13.98	13.70	14.11	15.35	14.76	14.96	14.12	15.09	15.20	15.19	15.11	15.27
K_2O	0.52	0.53	0.03	0.03	0.05	0.03	0.04	0.05	0.05	0.06	0.07	0.05	0.08	0.08
Total	91.09	90.91	91.45	90.64	91.90	89.98	89.76	89.62	88.52	89.99	89.57	89.27	89.05	89.52
Formula based on 6 (analcime) and 10 (natrolite) oxygen atoms														
Si	1.99	1.99	2.00	1.99	1.98	3.01	3.00	3.01	3.04	3.01	3.00	3.01	3.02	3.01
Al	1.01	1.02	1.00	1.02	1.03	2.03	2.05	2.03	2.02	2.03	2.03	2.03	2.01	2.02
Fe	0.00	0.00	0.00	0.00	0.00	0.00	0.00	0.00	0.00	0.00	0.00	0.00	0.00	0.00
Mg	0.00	0.00	0.00	0.00	0.00	0.00	0.00	0.00	0.00	0.00	0.00	0.00	0.00	0.00
Ca	0.00	0.00	0.00	0.00	0.00	0.00	0.00	0.00	0.00	0.01	0.01	0.00	0.00	0.00
Na	1.00	0.98	1.00	0.99	1.00	1.89	1.81	1.84	1.75	1.85	1.88	1.88	1.88	1.89
K	0.03	0.03	0.00	0.00	0.00	0.00	0.00	0.00	0.00	0.01	0.01	0.00	0.01	0.01

TABLE 8. Representative compositions of sodalite.

	1	2	3
SiO_2	37.19	36.53	36.41
Al_2O_3	31.07	31.52	31.20
FeO	0.01	0.02	0.01
CaO	0.01	0.11	0.11
Na_2O	25.20	25.14	25.12
K_2O	0.05	0.03	0.03
Cl	7.40	7.14	7.26
Total	100.92	100.49	100.13
Formula based on 21 oxygen atoms			
Si	6.04	5.96	5.98
Al	5.95	6.06	6.03
Fe	0.00	0.00	0.00
Ca	0.00	0.02	0.02
Na	7.93	7.95	7.99
K	0.01	0.01	0.01
Cl	2.04	1.97	2.02

magma having very low oxygen fugacity (Marks *et al.*, 2011 and references therein). In contrast to the other less-reduced rock types such as miaskitic nepheline syenites, or carbonatites, the low oxygen fugacity commonly results in enrichment in a CH_4-rich fluid phase in these rocks rather than a H_2O–CO_2-rich fluid (Andersen, 1990; Hansteen and Burke, 1990; Fall *et al.*, 2007; Schönenberger and Markl, 2008). The fractionating melts are enriched in Na, Cl, F and other volatile species as none are exsolved during the early magmatic stages. Such Na, Cl, F-rich melts have higher solubilites for high-field-strength elements (HFSE) such as Ti and Zr and eventually crystallize typomorphic minerals of the agpaitic systems such as eudialyte, låvenite, rinkite etc. (Sørensen, 1997; Markl and Baumgartner, 2002; Andersen *et al.*, 2010; Marks *et al.*, 2011). The agpaitic rocks have an extended crystallization interval and the near-solidus temperature can be as low as 500–400°C as seen in the late-crystallizing agpaitic veins in the Ilímaussaq complex (Markl and Baumgartner, 2002). However, there is undoubtedly a continuum to the hydrothermal stages. As a result it is difficult to differentiate between the early-, late- and post-magmatic (including subsolidus deuteric/hydrothermal alteration) assemblages in these rocks. The scenario becomes much more complex when these rocks suffer metamorphism and/or consanguineous metasomatism and deformation, leaving only part of the relict igneous characters both in terms of their mineral assemblages and textures.

The mineralogy of the Sushina agpaitic gneisses can be subdivided into: (1) the primary–late magmatic assemblage (feldspars + Ne-I + Cpx-I + rinkite + late-magmatic/Eud-I ± manganoan magnesio-arfvedsonite); (2) a subsolidus deuteric/hydrothermal alteration assemblage (Ne-II + microcline + Cpx-II ± post-magmatic/Eud-II ± sodalite ± pectolite – serandite ± catapleiite/gaidonnyaite ± hilairite ± *REE*-rich phases mainly cerianite-Ce, pyrochlore); (3) low-temperature alteration assemblage (analcime + natrolite). The paragenesis of these assemblages is discussed below.

Phase equilibria

The phase equilibria involving assemblage of clinopyroxene, nepheline and alkali feldspar provide estimates of the pressure, temperature and silica activity during successive stages of mineralogical evolution ranging from early- to late- and post-magmatic stages, respectively. The pressure estimate can be obtained considering the solid-solid reaction involving nepheline, albite and the jadeiitic component of clinopyroxene:

$$NaAlSi_3O_8(Ab) + NaAlSiO_4(Ne) = 2NaAlSi_2O_6(Jd) \quad (1)$$

Reaction 1 plotted in *P-T* space for appropriate activity values using *THERMOCALC* software of Holland and Powell (1998) shows that at 700°C the equilibration pressure will be 2.7 kbar. Considering the maximum stability field of the zeolite group of minerals present within the low-temperature assemblage involving analcime and natrolite pressure can be fixed at 3 kbar. Thus it can be presumed that the equilibrium pressure during successive stages of early- to late-magmatic and deuteric alteration was ~3 kbar. The temperature and silica activity during these above mentioned stages can be calculated from the reactions:

$$NaAlSiO_4(Ne) + SiO_2(aq) = NaAlSi_2O_6(Jd) \quad (2)$$
$$NaAlSiO_4(Ne) + 2SiO_2(aq) = NaAlSi_3O_8(Ab) \quad (3)$$
$$NaAlSi_2O_6(Jd) + SiO_2(aq) = NaAlSi_3O_8(Ab) \quad (4)$$

For undersaturated rocks consideration of silica activity as an aqueous phase is required for these reactions. For the calculation of end-member component activities from mineral formulae, the solution models of Holland and Powell (1998) was employed for the jadeite component of clinopyroxene and the activity of nepheline was calculated

https://doi.org/10.1180/minmag.2016.080.057 Published online by Cambridge University Press

TABLE 9. Representative compositions of biotite.

	1	2	3	4	5	6
SiO_2	36.24	35.75	36.28	36.40	36.05	35.90
TiO_2	0.54	0.45	0.47	0.41	0.54	0.52
Al_2O_3	19.85	20.36	19.80	18.90	20.56	18.41
FeO	8.90	8.79	8.83	11.51	8.69	12.03
MnO	11.02	11.14	10.91	10.97	11.12	10.81
MgO	8.65	8.15	8.89	7.40	8.90	7.75
CaO	0.00	0.00	0.00	0.00	0.00	0.00
Na_2O	0.00	0.00	0.00	0.00	0.00	0.00
K_2O	10.13	9.99	10.06	9.46	10.13	10.15
ZnO	1.45	1.46	1.32	1.43	1.42	1.28
H_2O*	3.97	3.94	3.97	3.92	4.00	3.91
Total	100.75	100.03	100.53	100.40	101.41	100.76
Formula based on 22 oxygen atoms						
Si	5.48	5.44	5.48	5.57	5.41	5.51
Al^{IV}	2.52	2.56	2.52	2.43	2.60	2.49
Al^{VI}	1.01	1.09	1.01	0.97	1.04	0.84
Ti	0.06	0.05	0.05	0.05	0.06	0.06
Fe	1.13	1.12	1.12	1.47	1.09	1.54
Mn	1.41	1.44	1.40	1.42	1.41	1.41
Mg	1.95	1.85	2.00	1.69	1.99	1.77
Zn	0.16	0.16	0.15	0.16	0.16	0.15
Y-Total	5.72	5.71	5.73	5.76	5.75	5.77
Ca	0.00	0.00	0.00	0.00	0.00	0.00
Na	0.00	0.00	0.00	0.00	0.00	0.00
K	1.95	1.94	1.94	1.85	1.94	1.99
X-Total	1.95	1.94	1.94	1.85	1.94	1.99
OH*	4.00	4.00	4.00	4.00	4.00	4.00
Total	19.67	19.65	19.67	19.61	19.69	19.76
Fe/Fe+Mg	0.37	0.38	0.36	0.47	0.35	0.47

*OH calculation is after Tindle and Webb (1990).

using Ghiorso (http://melts.ofm-research.org/MELTSapplet.html). As albite is pure, the unit activity of albite has been considered. The above reactions (# 2–4) plotted in an activity-corrected isobaric (3 kbar) T – a_{SiO_2} diagram (Fig. 9) using *THERMOCALC* software of Holland and Powell (1998) indicate an invariant equilibrium relation between these reactions, which was maintained throughout the successive stages.

The early magmatic crystallization conditions were determined using the compositions of non-aligned zoned clinopyroxenes (Cpx-I) and the least-altered nephelines (Ne-I) with largest amounts of excess silica, which corresponds to the highest temperature as deduced by Hamilton (1961) (Fig. 3*c*). Subsolidus deuteric/hydrothermal conditions were determined using partially-altered nepheline (Ne-II) compositions and Ae-Jd rich clinopyroxenes (Cpx-II) defining an incipient gneissosity without any associated eudialyte. Additionally, a second stage of a subsolidus deuteric condition was calculated using Cpx-II and Ne-II, particularly those which are associated with eudialyte (Eud-II) and related alteration assemblage of pectolite–serandite, hilairite, catapleiite/gaidonnyaite and cerianite-(Ce).

Primary- to late-magmatic assemblage

The primary magmatic mineral assemblage is represented mainly by the nepheline (Ne-I) present either as inclusions or relict phenocrysts, feldspars and diopsidic pyroxenes (Cpx-I). On the basis of

https://doi.org/10.1180/minmag.2016.080.057 Published online by Cambridge University Press

TABLE 10. Representative compositions of spessartine.

	1	2
SiO_2	37.83	37.05
TiO_2	0.00	0.00
Al_2O_3	21.03	20.97
FeO	2.73	2.08
MnO	40.89	40.46
MgO	0.00	0.00
CaO	0.87	0.74
Total	103.35	101.30
Formula based on 12 oxygen atoms		
Si	3.01	3.00
Ti	0.00	0.00
Al	1.97	2.00
Fe^{3+}	0.00	0.00
Fe^{2+}	0.18	0.16
Mn	2.76	2.77
Mg	0.00	0.00
Ca	0.07	0.06
mol.% end-members		
Almandine	6.0	5.4
Spessartine	91.6	92.5
Pyrope	0.0	0.0
Grossular	2.5	2.2
Andradite	0.0	0.0
Uvarovite	0.0	0.0

nepheline thermometry it has been estimated that the least-altered nephelines (Ne-I) were equilibrated at *c.* 700°C (Fig. 3*c*) and considered to be the lowest temperature of crystallization of the precursor agpaitic nepheline syenite. The early-magmatic assemblages involving Ne-I and Cpx-I plotted in a $T - a_{SiO_2}$ diagram (Fig. 9) corroborates this temperature estimate ($T = 726$°C, $a_{SiO_2} = 0.60$). However, this temperature cannot be constrained using two feldspar thermometry due to the pure end-member compositions of alkali feldspars (albite and orthoclase) without any significant anorthite component. Pure end-member compositions of albite and orthoclase can be interpreted as a primary magmatic signature similar to that of the litchfieldite, a variety of subsolvus nepheline syenite (Mitchell, 1996; Platt, 1996). However, considering the subsolidus assemblages formed after eudialyte decomposition, we consider that the Sushina syenites are subsolidus nepheline syenites which have suffered extensive subsolidus re-equilibration below 500°C (discussed below). The presence of microcline at orthoclase grain boundaries could be either due to incomplete metamorphic re-equilibration or due to post-magmatic microclinization during subsolidus alteration. Zoned pyroxene (Cpx-I) with a planar boundary between core and rim of diopside – hedenbergite composition is characteristic of the primary magmatic pyroxene without any appreciable amount of jadeite and aegirine (Fig. 4*b*). Evolution of these pyroxenes from a diopsidic core to an aegirine rim (Fig. 4*a*) is a feature of primary magmatic pyroxenes in alkaline rocks (Platt, 1996; Vuorinen *et al.*, 2005; Mitchell and Liferovich, 2006; Fall *et al.*, 2007; Marks *et al.*, 2008). Moreover, the presence of Cpx-I as inclusions within the late-formed Mn-rich magnesio-arfvedsonite (Fig. 8) also indicates formation of these pyroxenes during the

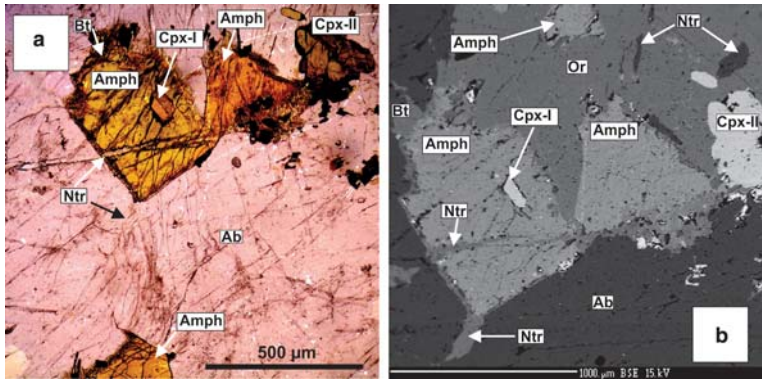

FIG. 8. Rare occurrence of arfvedsonitic amphibole (Amph) containing inclusion of Cpx-I in association with Cpx-II, orthoclase (Or) and albite (Ab) shown in plane-polarized light (*a*) and BSE image (*b*). Note that these alkali amphiboles are marginally-altered to biotite (Bt). The later paragenesis of natrolite (Ntr) is evident from its occurrence as thin veins rimming and cutting across the alkali amphiboles.

https://doi.org/10.1180/minmag.2016.080.057 Published online by Cambridge University Press

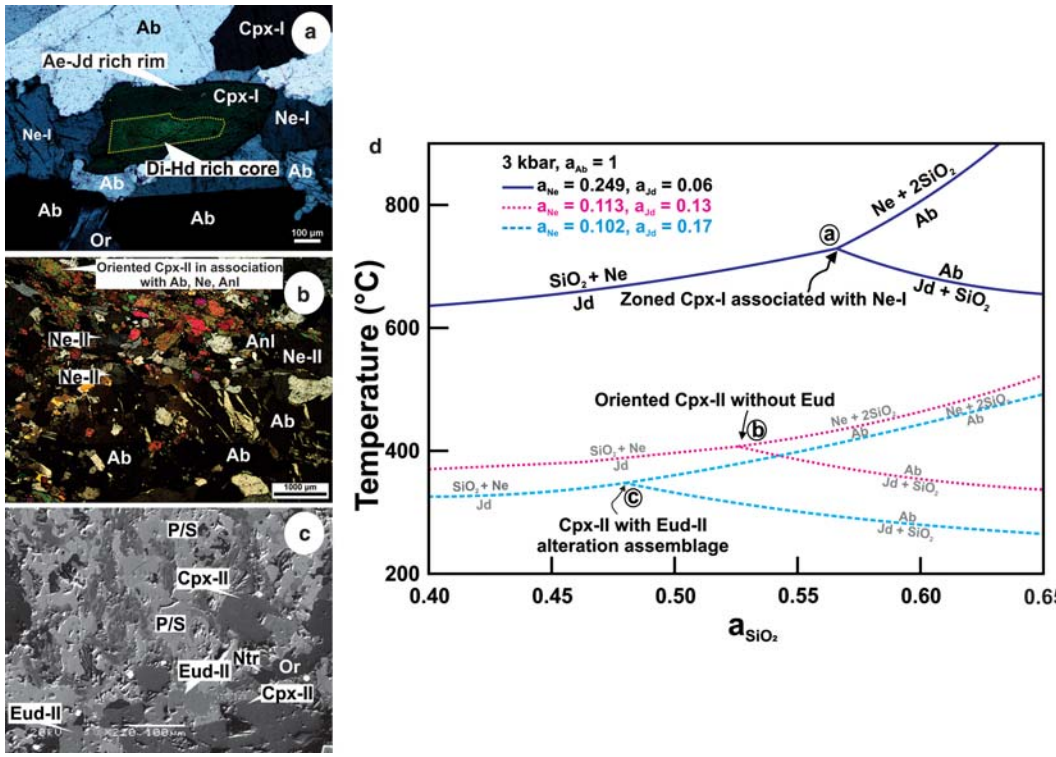

FIG. 9. Phase diagram related to various textural assemblages involving different generations of clinopyroxene and nepheline from magmatic to deuteric subsolidus stages for Sushina agpaitic syenites (See text for discussion).

early stages of magmatic crystallization compared to late-formed amphibole. Thus, paragenetically Cpx-I is considered as primary magmatic in nature. This is in agreement with the recent study of Giehl *et al.* (2013) which demonstrate that reduced and dry conditions promotes crystallization of nepheline, alkali feldspars, hedenbergite-rich clinopyroxene, fayalite-rich olivine with minor amounts of ulvospinel-rich magnetite as found in a peralkaline phonolitic dyke in the Ilímaussaq complex, Greenland. However, the absence of olivine in the Sushina agpaitic rocks indicates that the parent melt was not reduced to the extent of the parent phonolitic melt of the Ilímaussaq complex and more evolved inhibiting magnetite and olivine crystallization (Giehl *et al.*, 2014).

Long needle-like rinkite inclusions within the late magmatic Mn-rich eudialyte (Fig. 7) indicate that these predate eudialyte (Chakrabarty *et al.*, 2013), and are the first typomorphic minerals crystallized from the parent melt. This is in agreement with the observation that Cl partitioning is preferred in the fluid phase relative to F resulting in the crystallization of the rinkite (Aiuppa, 2009; Giehl *et al.*, 2014) during early magmatic stages.

Subsolidus deuteric/hydrothermal alteration assemblage

The subsolidus deuteric or hydrothermal alteration assemblage is represented mainly by the post-magmatic eudialyte (Eud-II) and its decomposition assemblages (both Eud-I and II). No veins or pegmatites having similar mineralogical compositions to those of the host agpaitic gneisses were observed in and around the Sushina Hill complex, and we consider that the fluid responsible for eudialyte paragenesis, as well its decomposition, was essentially a system-derived deuteric fluid. Mesh-like textures related to Mn-rich eudialyte-II engulfing and corroding early-formed pyroxene (Cpx-II) are believed to be the characteristic textural feature which indicates that the Eud-II was formed late in the paragenetic sequence compared to Cpx-II (Fig. 4*c*). In general such

https://doi.org/10.1180/minmag.2016.080.057 Published online by Cambridge University Press

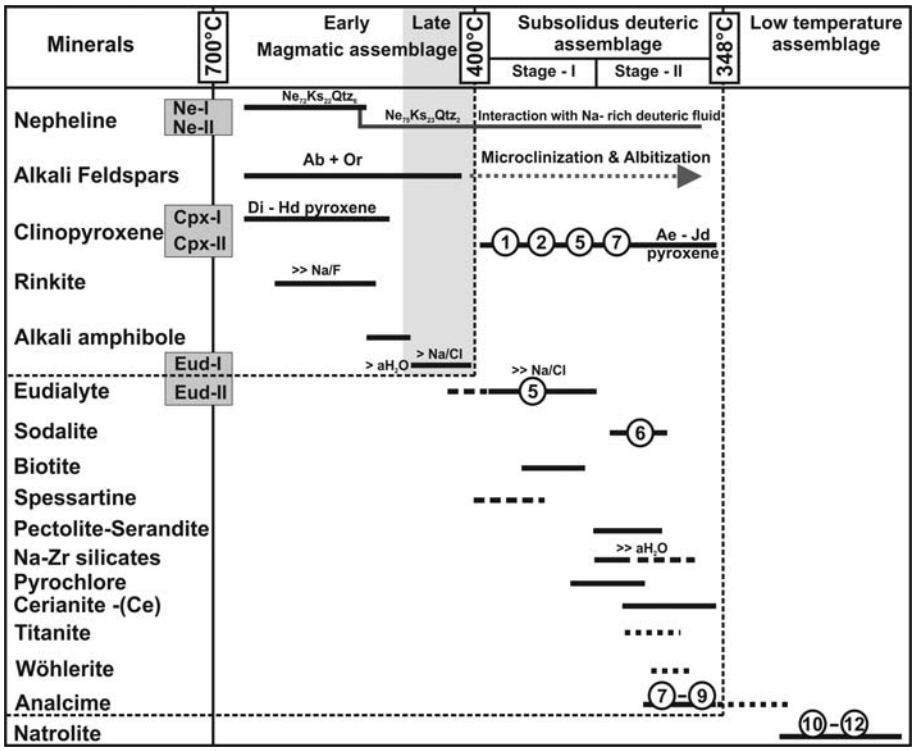

FIG. 10. A generalized paragenetic sequence for the Sushina syenites illustrating the magmatic, subsolidus, metamorphic and a very low-temperature assemblages as deduced from the textural relationships and compositions of the minerals of the eudialyte-nepheline syenites. Numbers marked in Arabic numerals indicate possible reaction(s) of formation of the individual species. (See text for discussion).

Mn-rich eudialyte usually forms during late- to post-magmatic stages in agpaitic nepheline syenites (Schilling *et al.*, 2011*a*; Chakrabarty *et al.*, 2012; Mitchell and Chakrabarty, 2012). The onset of eudialyte crystallization requires an elevated Cl and Zr content of the evolving melt/fluid (Giehl *et al.*, 2014). The absence of zircon and paucity of alkali amphiboles in the agpaitic gneisses further substantiate that eudialyte was probably formed by the following NaCl consuming reaction as described by Marks *et al.* (2011):

$$3\text{Zrn} + 0{\cdot}75\text{Arfv} + 0{\cdot}25\text{H}_2\text{O} + \text{NaCl} + 18{\cdot}5\text{SiO}_2 + 6\text{CaO} + 6{\cdot}25\text{Na}_2\text{O} = \text{Eud-II} + 0{\cdot}75\text{Aeg} \quad (5)$$

(Zrn: zircon; Arfv: arfvedsonite; Eud: eudialyte and Aeg: aegirine).

This reaction also successfully explains crystallization of more aegirine-rich pyroxenes (up to 87 mol.% in Cpx-II, Table 3) at the expense of arfvedsonitic amphibole during the late- to post-magmatic stage in association with Eud-II. This can be further substantiated by the low concentration of Fe in the eudialyte (Eud-I & II) as the majority of the Fe was consumed during the formation of the pyroxenes and alkali amphibole. In most nepheline syenite complexes it has been determined that following an initial enrichment in hedenbergite component, the pyroxenes became progressively enriched in Na and Fe^{3+} leading to formation of aegirine (Platt, 1996). This enrichment can arise at any point in the evolutionary trend from diopside- to hedenbergite-rich compositions. This in turn implies that during the course of evolution, the fluid phase associated with the parent melt became progressively persodic and more reduced giving rise to precipitation of arfvedsonitic amphibole, aegirine and post-magmatic eudialyte (Eud-II) (Markl *et al.*, 2010). As the Na/(Na + Ca) ratio of the fluid increases with decreasing temperature, the Ca-bearing clinopyroxene (diopside) becomes

https://doi.org/10.1180/minmag.2016.080.057 Published online by Cambridge University Press

unstable and precipitation of Na-rich clinopyroxene (aegirine) was enhanced at a lower temperature (Giehl *et al.*, 2014). This is in agreement with the observed phase assemblage between Ne-II and Cpx-II defining an incipient gneissosity without associated eudialyte indicating an equilibration temperature of 405°C with a_{SiO_2} decreasing to 0.52 compared to the early- to late-magmatic stage (Fig. 9).

Crystallization of eudialyte marks an increased H_2O activity in the fluid. This is reflected in the decomposition assemblage formed after eudialyte (Mitchell and Chakrabarty, 2012) which is represented mainly by various hydrated sodium zirconium silicates such as catapleiite/gaidonnyaite and hilairite, together with pectolite–serandite, pyrochlore, cerianite-(Ce) and wöhlerite (Mitchell and Chakrabarty, 2012; Chakrabarty *et al.*, 2013; Mahato *et al.*, 2013). The stability of the naturally-occurring pectolite is estimated to be in the range of 359–250°C (Karup-Møller, 1969; Dutrow *et al.*, 2001). This is in agreement with the calculated equilibration temperature of 348°C at a_{SiO_2} = 0.48 involving Cpx-II, Ne-II found within the eudialyte alteration assemblages of pectolite–serandite, catapleiite/gaidonnyaite and cerianite-(Ce) (Fig. 9). Cerianite-(Ce), marks a change in the pH condition from more basic towards acidic, i.e. prevalence of oxidizing condition during the later stages of the fluid evolution. This further confirms that the eudialyte decomposition invariably took place above 400°C as proposed by Chakrabarty *et al.* (2013). Compared to other agpaitic complexes, the Sushina agpaitic gneisses are characterized by limited occurrence of sodalite. Textural features indicate that sodalite is only formed where decomposing eudialyte released Cl and reacted with adjacent nepheline by the reaction

$$6NaAlSiO_4(\text{nepheline}) + 2NaCl(\text{fluid}) = Na_8Al_6Si_6O_{24}Cl_2(\text{sodalite}) \quad (6)$$

These partially-altered nephelines (Ne-II) with immediate contact to sodalite and zeolite-group minerals (analcime and natrolite) approach the Buerger ideal stoichiometric composition of nepheline (Fig. 3). However, Ne-II cannot be considered as part of the subsolidus deuteric alteration assemblage as they formed during a primary magmatic stage. Perchuk and Ryabchikov (1968) demonstrated that alkaline rocks are susceptible to very low-temperature syngenetic metasomatic processes including microclinization of high temperature orthoclase and albitization. If this occurs below 500°C, feldspar will be near end-member composition and nepheline will approach the Morozewicz–Buerger convergence field. This is in accordance with the observed temperature window between 405°C and 348°C demonstrating that subsolidus alteration might have taken place below 500°C. In general, decomposition of eudialyte to pectolite–serandite and various sodian-zirconosilicates (catapleiite/gaidonnyaite and hilairite) indicate an increase in a_{H2O} and in such conditions sodalite is unstable (Giehl *et al.*, 2014). This explains successfully the paucity of sodalite in the Sushina agpaitic rocks within the deuteric/hydrothermal assemblage. Moreover, the abundance of water-rich sodian-zirconosilicates in accord with the theoretical phase diagrams of Andersen *et al.* (2010) suggests that catapleiite should replace zircon and eudialyte at higher H_2O activities. Increasing activity of water can also be substantiated by the replacement of pyroxene and amphibole by late-formed manganoan biotite.

Spessartine is a less common species among the garnet group of minerals, and metasomatic spessartine is reported from many granites and aplites. The best example is the South Mountain Batholith, Nova Scotia where it was formed between 500°C and 550°C (Kontak and Corey, 1988). Synthetic spessartine can be produced readily in the range of 410–900°C at 0.5–3 kbar water pressure but becomes increasingly hydrated at temperatures >600°C (Deer *et al.*, 1992). Spessartine formation requires elevated concentrations of Mn and Al. Crystallization of Mn rich eudialyte during the late – post magmatic stage facilitate such conditions and spessartine was probably formed under these conditions. Moreover, our data do not correspond to the hydrated nature of the spessartine and can be assumed that the spessartine was formed close to 400°C.

Overall the magmatic and subsolidus assemblages are quite similar to those found in the arfvedsonite-bearing nepheline syenite (lakarpite) and eudialyte-catapleiite-bearing nepheline syenite (grennaite) at the Norra Kärr agpaitic complex. The remnant patches of magnesio-arfvedsonite together with albite, orthoclase and nepheline shielded by the assemblage of more-deformed eudialyte-catapleiite-aegirine-bearing syenite at Sushina are very similar to those found at the Norra Kärr complex. A similar feature is also observed at the Red Wine complex, where more-deformed and metasomatized gneisses girdle less-deformed eudialyte-bearing agpaitic nepheline syenites in which relict igneous textures are preserved.

https://doi.org/10.1180/minmag.2016.080.057 Published online by Cambridge University Press

Origin of aegirine–jadeite (Ae–Jd)-rich pyroxene

The origin and stabilization of the aegirine–jadeite-rich Cpx-II merits further discussion in the present study in context to similar occurrences in metamorphosed alkaline complexes of Norra Kärr (Adamson, 1944), Red Wine (Curtis and Gittins, 1979) and Nkonglong (Kornprobst *et al.*, 1976) in comparison to unmetamorphosed aegirine lljavrite of the Ilímaussaq alkaline complex (Markl *et al.*, 2001). It has been argued that in metamorphosed agpaitic complexes, amphibolite-facies metamorphism leads to formation of an Ae–Jd pyroxene, whereas miaskitic rocks are characterized by the formation of aluminian aegirine-augite and omphacitic pyroxene (Woolley *et al.*, 1996). However, other than Ae–Jd pyroxene no other metamorphic minerals were reported from these localities. As discussed earlier, at Norra Kärr clinopyroxene in highly schistose grennaite is more jadeiitic ($Ae_{61}Jd_{39}$–$Ae_{81}Jd_{18}$) than non-schistose lakarpite ($Ae_{82}Jd_{10}$–$Ae_{78}Jd_{11}$) and zoned clinopyroxene of the grennaite show jadeite enrichment from core to rim ($Ae_{86}Jd_{12} \rightarrow Ae_{65}Jd_{34}$) (Mitchell, unpublished data) (Fig. 5*a*). However, preservation of natrolite, pectolite within grennaite and lakarpite, probably indicate a metasomatic event at a late stage consanguineous with Mn-rich eudialyte precipitation from the metasomatic fluid. In contrast, zoned clinopyroxenes of the Two Tom Lake and Red Wine complexes show a completely reversed trend, i.e. jadeiitic core and aegirine-rich rim ($Ae_{29}Jd_{68} \rightarrow Ae_{58}Jd_{36}$) (Mitchell, unpublished data) (Fig. 5*b*). Furthermore, aegirine in lujavrite from the metamorphism-free Ilímaussaq alkaline complex in general contains 6–7 mol.% of jadeite and may reach up to $Ae_{72}Jd_{25}$ (Type 3-Cpx, Markl *et al.*, 2001) (Fig. 5*c*). Thus, it is not obvious that metamorphism of agpaitic rocks can lead to the formation of Ae–Jd pyroxene. In general, pure jadeite is a characteristic mineral for the rocks of blueschist-facies metamorphism. However, jadeite can be formed in a silica deficient environment at a pressure of ≤5 kbar with temperature *c*. 700–350°C by the reactions # 1–2 depending on the activity of silica (Yoder and Weir, 1951; Adams, 1953; Robertson *et al.*, 1957; Coleman, 1961; Hlabse and Kleppa, 1968; Markl *et al.*, 2001). This jadeite component can be incorporated into clinopyroxene by a jadeite-like substitution at relatively low pressure in silica-undersaturated rocks by a model reaction which can be approximated as

$$\text{`Clinpyroxene'} + NaAlSi_2O_6 = \text{Na-Al-rich pyroxene} \quad (7)$$

(Bell and Kalb, 1969; Popp and Gilbert, 1972; Upadhyay, 2012). At lower temperatures with increasing water activity reaction 1 may promote analcime formation rather than jadeite. This indicates that the formation of jadeite essentially took place under water-deficient high-temperature conditions at least above the temperature of zeolite-facies metamorphism (>250°C), and in accord with the calculated equilibration temperature of 348°C where both analcime and Ae–Jd pyroxene were in equilibrium as observed in this study. Schilling *et al.* (2011*b*) also reported the formation of Ae–Jd pyroxene at subsolidus conditions from a low-silica fluid at a temperature *c*. 500°C from the Mont Saint Hilaire Complex. This clearly demonstrates that the jadeite formation and subsequent incorporation in clinopyroxene can occur during metasomatism involving a highly alkaline and low-silica fluid at relatively low pressure and temperature. This is in agreement with the jadeite enrichment at relatively low a_{SiO_2} (0.52–0.48) during a subsolidus deuteric stage compared to an early- to late-magmatic stage (0.60) within a temperature window of 400–348°C at Sushina. Moreover, retention of pectolite within the eudialyte decomposition assemblage could move the stability field of pectolite–serandite up to at least 400°C. This is also in accord with the estimated temperature of eudialyte decomposition at *c*. 400°C under highly alkaline conditions at Sushina (Chakrabarty *et al.*, 2013). The entire *P–T* window starting from the early- to late-magmatic through subsolidus deuteric stages overlap with the greenschist–lower-amphibolite facies of metamorphism and consanguineous deformational event in the agpaitic rocks of the Sushina Hill Complex. This further implies that the incorporation of the jadeiitic component in pyroxene could be related to an extended subsolidus process at very low temperature (up to 348°C) rather than as a metamorphic process as described earlier (Goswami and Basu, 2013). It is most probable that during such a relatively low-temperature process, any accompanying deformation could result in preferential alignment of the mafic (pyroxene) and felsic minerals

https://doi.org/10.1180/minmag.2016.080.057 Published online by Cambridge University Press

(feldspars), eventually resulting in an overall gneissosity in these rocks.

Low-temperature assemblage

The zeolite group of minerals are represented by analcime and natrolite. Textural investigation reveals that analcime is mainly restricted to the nepheline–albite grain boundaries while natrolite is more pervasive and found to be replacing nepheline, albite and in places sodalite (Figs 3 and 6*d*). Analcime is found to be formed at the expense of nepheline and albite (Fig. 3*a*) through the probable reactions

$$NaAlSiO_4(Ne) + NaAlSi_3O_8(Ab) + H_2O = 2NaAlSi_2O_6 \cdot H_2O(Anl) \quad (8)$$

$$NaAlSi_3O_8(Ab) + H_2O = NaAlSi_2O_6 \cdot H_2O(Anl) + SiO_2(aq) \quad (9)$$

$$NaAlSiO_4(Ne) + SiO_2(aq) + H_2O = NaAlSi_2O_6 \cdot H_2O(Anl) \quad (10)$$

Fluids which are responsible for the precipitation of zeolite-group minerals can be either the same deuteric fluid which caused eudialyte decomposition or originate from an extraneous source. Analcime can form at higher temperature relative to natrolite as found in blairmorites, where analcime macrocrysts are formed at 500°C (Henderson *et al.*, 2014). This seems reasonable as analcime is found to be associated with nepheline (Ne-II) and Ae–Jd pyroxene (Cpx-II) at subsolidus temperature between 400°C and 348°C with nepheline and albite. This probably continued beyond 348°C as analcime is found within the decomposition assemblage formed after eudialyte. Considering the greenschist- to lower-amphibolite-facies metamorphism around the Sushina Hill complex, it can be inferred that natrolite formation came last in the mineral paragenesis and well after the peak metamorphic event. With further decreasing temperature (<348°C) natrolite becomes stable together with analcime at the expense of nepheline and albite through the reactions:

$$2NaAlSiO_4(Ne) + SiO_2(aq) + 2H_2O(aq) = Na_2Al_2Si_3O_{10} \cdot 2H_2O(Ntr) \quad (11)$$

$$2NaAlSi_3O_8(Ab) + 2H_2O = Na_2Al_2Si_3O_{10} \cdot 2H_2O(Ntr) + 3SiO_2(aq) \quad (12)$$

$$2NaAlSi_2O_6 \cdot H_2O(Anl) = Na_2Al_2Si_3O_{10} \cdot 2H_2O(Ntr) + SiO_2(aq) \quad (13)$$

In contrast, Schilling *et al.* (2011*b*) reported that natrolite is the sole zeolite mineral stable at lower temperature (250°C) and analcime forms later in these parageneses below 150°C. This implies that at lower temperatures the analcime stability field will expand at the expense of natrolite (see fig. 19d of Schilling *et al.* 2011*b*). However, at Sushina, natrolite veins dominant over analcime, not only in the agpaitic unit, but also in the associated miaskitic and albitite, cross-cutting all precursor aluminosilicates (Mahato *et al.* 2013). This is in agreement with late-stage paragenesis of natrolite compared to analcime at further low temperatures, a case similar to the Pilansberg complex (Mitchell and Liferovich, 2006).

As this stage may be characterized by infiltration of an external fluid of diverse composition indicating an open system behaviour, it is not pertinent to construct phase diagrams for this late stage without characterizing the nature and composition of this fluid.

Conclusion

Our investigation of the magmatic, subsolidus deuteric/hydrothermal and further low-temperature assemblage in the Sushina agpaitic gneisses yields the following conclusions which are summarized in Fig. 10. The parent melt of the precursor agpaitic syenite was enriched in volatiles such as Cl, F together with LILE and HFSE, resulting in the formation of primary magmatic nepheline, alkali feldspars, diopsidic pyroxene (Cpx-I), rinkite and late-magmatic eudialyte (Eud-I). The estimated lowest temperature of crystallization was found to be ~700°C. With decreasing temperature the primary magmatic assemblage has undergone extensive subsolidus low-temperature (~400°C) equilibration with Na- and Cl-rich deuteric fluid causing superposition of the subsolidus assemblage over the magmatic assemblage. The initial stage of the subsolidus assemblage (Stage – I, Fig. 10) is characterized by the precipitation of post-magmatic eudialyte (Eud-II) and aegirine–jadeite-rich clinopyroxene (Cpx-II) from the evolving deuteric fluid. The onset of eudialyte crystallization marks an increase in the Na/Cl ratio of the deuteric fluid and together with activity of H_2O and represents an increasing alkalinity stage. The next stage (Stage – II, Fig. 10) of the subsolidus alteration is represented by the decomposition assemblages formed after eudialyte. Formation of pectolite–serandite together with diverse sodian-zirconosilicates at this

https://doi.org/10.1180/minmag.2016.080.057 Published online by Cambridge University Press

stage indicates an increase in the water activity of the evolving deuteric fluid. Precipitation of cerianite-(Ce) at lower (~348°C) temperature marks a change in pH condition and in redox conditions from reducing to oxidizing. This stage can be described as a decreasing alkalinity stage. The entire assemblage of the magmatic-to-subsolidus deuteric stage is well within the range of calculated temperature 700°C–348°C and hence the entire assemblage is retained even after undergoing greenschist to lower-amphibolite metamorphism at Sushina. However, retention of low-temperature assemblages represented by the natrolite probably indicate retrogressive phases of this metamorphic event or continuation of the subsolidus process below 250°C. The source of this very late-stage fluid cannot be identified conclusively due to lack of stable isotope data. However, increasing silica content in the fluid probably indicates that the fluid might be derived from an external source and different from the deuteric fluid.

Due to the overlapping relationship between the magmatic-to-subsolidus process and consanguineous metamorphic-deformational event, gneissosity is developed within these rocks, but they have retained the majority of their igneous textures such as zoned diopsidic clinopyroxene with planer boundaries separating core and rim, and most importantly an overall megacrystal-to-hypidiomorphic granular texture. Our study demonstrates successfully that metamorphism of agpaitic rocks up to lower-amphibolite facies does not perturb the decomposition assemblage formed after eudialyte. This is possible only when the deuteric fluid itself acted as an agent for metamorphism and retained the majority of the subsolidus assemblages making distinction difficult between the magmatic and metamorphic mineral assemblages in metamorphosed agpaitic rocks. Furthermore, the gneissose, folded and sheared character of the Sushina agpaitic syenites correspond to the deformed nature of the complex. We emphasize the usage of the terminology 'metamorphosed' with caution for the Sushina agpaitic syenites as they lack true metamorphic assemblages. Because of the resemblance between the agpaitic rocks at Sushina and Norra Kärr in terms of mineralogical and textural features, our hypothesis could be extended to the latter complex which is considered in the literature as a metamorphosed peralkaline complex. An extensive metasomatized zone around most of the metamorphosed peralkaline complexes (Red Wine, Norra Kärr) is noteworthy and requires an in-depth re-examination in terms of magmatic-hydrothermal and metamorphic assemblages to decipher the extent and effect of these individual processes for these complexes.

Acknowledgements

This work is supported by the Department of Science and Technology (DST), India through a Fast Track Research Scheme (SR/FTP/ES-65/2013) awarded to AC. R. H. Mitchell's work on alkaline rocks is supported by the Natural Sciences and Engineering Research Council of Canada. The manuscript has benefitted from many rounds of discussions with Axel Sjöqvist, Rajib Kar, Supriyo Pal and Sudipta Chakrabarty. We are thankful to the reviewers for their thought provoking and constructive suggestions which helped to enhance the clarity of this communication. The editorial care of Prof. Peter Williams and Dr. Katharina Pfaff is highly appreciated.

References

Adams, L.H. (1953) A note on the stability of jadeite. *American Journal of Science*, **251**, 299–308.

Adamson, O.J. (1944) The petrology of the Norra Kärr district. *Geologiska Föreningen Stockholm Førhandlingar*, **66**, 113–255.

Aiuppa, A. (2009) Degassing of halogens from basaltic volcanism: insights from volcanic gas observations. *Chemical Geology*, **263**, 99–109.

Aksenov, S.M., Rastsveteva, R.K., Mitchell, R.H. and Chakrabarty, A. (2014) Crystal Structure of Manganese-Rich variety of Eudialyte from Sushina Hill, India and Manganese Ordering in Eudialyte-group Minerals. *Crystallography Reports*, **59**, 146–154.

Andersen, T. (1990) Melt-mineral-fluid interaction in peralkaline silicic intrusion in the Oslo rift, Southeast Norway. IV: fluid inclusions in the Sande nordmarkite. *Norges Geologiske Undersøkelse Bulletin*, **417**, 41–54.

Andersen, T., Erambert, M., Larsen, A.O. and Selbekk, R. S. (2010) Petrology of nepheline syenite pegmatites in the Oslo Rift, Norway: zirconium silicate mineral assemblages as indicators of alkalinity and volatile fugacity in mildly agpaitic magma. *Journal of Petrology*, **51**, 2303–2325.

Armstrong, J.T. (1991) Quantitative elemental analysis of individual microparticles with electron beam instruments. Pp. 261–315 in: *Electron Probe Quantification* (K.F.J. Heinrich and D.E. Newbury, editors). Plenum Press, New York & London.

Basu, S.K. (1993) Alkaline-Carbonatite Complex in Precambrian of South Purulia Shear Zone, Eastern India: its characteristics and mineral potentialities. *Indian Minerals*, **47**, 179–194.

Bell, P.M. and Kalb, K. (1969) *Stability of Omphacite in the Absence of Excess Silica.* Carnegie Institute

https://doi.org/10.1180/minmag.2016.080.057 Published online by Cambridge University Press

Washington, Annual Report, Directory Geophysics Laboratory 1967–1968, 97–98.

Chakrabarty, A. (2009) *Petrogenesis of carbonatite and associated alkaline rocks, Purulia, W.B., India*. PhD Thesis, Department of Earth Sciences, Indian Institute of Technology Roorkee, India.

Chakrabarty, A. and Sen, A.K. (2010) Enigmatic association of the carbonatite and alkali-pyroxenite along the Northern Shear Zone: a saga of primary magmatic carbonatites. *Journal of Geological Society of India*, **74**, 403–413.

Chakrabarty, A. and Sen, A.K. (2013) Geochronological constraints and tectonic implications of the alkaline rocks of South Purulia Shear Zone, W.B., India. Pp. 86–88. in: *18th Convention of Indian Geological Congress & International Symposium "Minerals and Mining in India-The way forward, inclusive of cooperative mineral-based industries in SAARC countries" (extended Abstract)*.

Chakrabarty, A., Sen, A.K. and Ghosh, T.K. (2009) Amphibole – A key indicator mineral for petrogenesis of carbonatite from Purulia, West Bengal, India. *Mineralogy and Petrology*, **95**, 105–112.

Chakrabarty, A., Pruseth, K.L. and Sen, A.K. (2011) First report of eudialyte occurrence from the Sushina hill region, Purulia district, West Bengal. *Journal of Geological Society of India*, **77**, 12–16.

Chakrabarty, A., Pruseth, K.L. and Sen, A.K. (2012) Composition and petrogenetic significance of the eudialyte group of minerals from Sushina, Purulia, West Bengal. *Journal of Geological Society of India*, **79**, 449–459.

Chakrabarty, A., Mitchell, R.H., Ren, M., Sen, A.K. and Pruseth, K.L. (2013) Rinkite, cerianite-(Ce), and hingganite-(Ce) in syenite gneisses from the Sushina Hill Complex, India: occurrence, compositional data petrogenetic significance. *Mineralogical Magazine*, **77**, 3137–3153.

Chatterjee, N. and Ghose, N.C. (2011) Extensive Early Neoproterozoic high-grade metamorphism in North Chotanagpur Gneissic Complex of the Central Indian Tectonic Zone. *Gondwana Research*, **20**, 362–379.

Chatterjee, N., Crowley, J.L. and Ghose, N.C. (2008) Geochronology of the 1.55 Ga Bengal anorthosite and Grenvillian metamorphism in the Chotanagpur gneissic complex, eastern India. *Precambrian Research*, **161**, 303–316.

Chatterjee, N., Banerjee, M., Bhattacharya, A. and Maji, A.K. (2010) Monazite chronology, metamorphism–anatexis and tectonic relevance of the mid-Neoproterozoic Eastern Indian Tectonic Zone. *Precambrian Research*, **179**, 99–120.

Coleman, R.G. (1961) Jadeite deposits of the Clear Creek area, New Idria District, San Benito County, California. *Journal of Petrology*, **2**, 209–247.

Curtis, L.W. and Gittins, J. (1979) Aluminous and titaniferous clinopyroxenes from regionally metamorphosed agpaitic rocks in central Labrador. *Journal of Petrology*, **20**, 165–186.

Deer, W.A., Howie, R.A. and Zussman, J. (1992) *An Introduction to Rock-forming Minerals.* Longman Scientific and Technical, England, pp. 31–46.

Droop, G.T.R. (1987) A general equation for estimation of Fe^{3+} concentrations in ferromagnesian silicates and oxides from microprobe analyses using stoichiometric criteria. *Mineralogical Magazine*, **51**, 431–435.

Duke, N.A. and Edgar, A.D. (1977) Petrology of the Blue Mountain and Bigwood felsic alkaline complexes of the Grenville province of Ontario. *Canadian Journal of Earth Sciences*, **14**, 515–538.

Dutrow, B.L., Travis, B.J., Gable, C.W. and Henry, D.J. (2001) Coupled heat and silica transport associated with dyke intrusion into sedimentary rock: effects on isotherm location and permeability evolution. *Geochimica et Cosmochimica Acta*, **65**, 3749–3767.

Fall, A., Bodnar, R.J., Szabó, C. and Pál-Molnár, E. (2007) Fluid evolution in the nepheline syenites of the Ditrău Alkaline Massif, Transylvania, Romania. *Lithos*, **95**, 331–345.

Floor, P. (1974) Alkaline gneisses. Pp. 124–142 in: *The Alkaline Rocks* (H. Sørensen, editor). John & Wiley, New York.

Giehl, C., Marks, M. and Novak, M. (2013) Phase relations and liquid line of descent of an iron-rich peralkaline phonolitic melt: an experimental study. *Contributions to Mineralogy and Petrology*, **165**, 283–304.

Giehl, C., Marks, M.A.W. and Novak, M. (2014) An experimental study on the influence of fluorine and chlorine on phase relations in peralkaline phonolitic melts. *Contributions to Mineralogy and Petrology*, **167**, 1–21.

Goswami, B. and Basu, S.K. (2013) Metamorphism of Proterozoic agpaitic nepheline syenite gneiss from North Singhbhum Mobile Belt, eastern India. *Mineralogy and Petrology*, **107**, 517–538.

Hamilton, D.L. (1961) Nephelines as crystallization temperature indicators. *Journal of Geology*, **69**, 321–329.

Hansteen, T.H. and Burke, E.A.J. (1990) Melt-mineral-fluid interaction in peralkaline silicic intrusions in the Oslo Rift, Southeast Norway; II, High-temperature fluid inclusions in the Eikeren-Skrim complex. *Norges Geologiske Undersøkelse Bulletin*, **417**, 15–32.

Harris, C. and Rickard, R.S. (1987) Rare-earth-rich eudialyte and dalyite from a peralkaline granite dyke at Strumsvola, Dronning Maud Land, Antarctica. *The Canadian Mineralogist*, **25**, 755–762.

Henderson, C.M.B., Hamilton, D.L. and Waters, J.P. (2014) Phase equilibrium in $NaAlSiO_4$ – $KAlSiO_4$ – SiO_2 – H_2O at 100 MPa pressure: equilibrium leucite composition and the enigma of primary analcime in

https://doi.org/10.1180/minmag.2016.080.057 Published online by Cambridge University Press

blairmortites revisited. *Mineralogical Magazine*, **78**, 171–201.

Hlabse, T.H. and Kleppa, O.J. (1968) The thermochemistry of jadeite. *American Mineralogist*, **53**, 1281–1292.

Holland, T.J.B. and Powell, R. (1998) An internally consistent thermodynamic data set for phases of petrologic interest. *Journal of Metamorphic Geology*, **16**, 309–343.

Holm, R.F. (1971) Some garnets, pyroxenes and amphiboles from nepheline gneisses in Ghana. *American Mineralogist*, **56**, 2111–2122.

Iwasaki, M. (1960) Clinopyroxenes intermediate between jadeite and aegirine from Suberidani, Tokusima Prefecture. *Journal Geological Society of Japan*, **66**, 334–340.

Karup-Møller, S. (1969) Xonotlite-, pectolite- and natrolite-bearing fracture veins in volcanic rocks from Nuussuaq, West Greenland. *Gronlnads Geologiske Undersøgelse*, **80**, 4–20.

Khomyakov, A. (1995) *Mineralogy of Hyperagpaitic Alkaline Rocks.* Clarendon Press, Oxford, UK, 222 pp.

Koark, H.J. (1960) Zum gefügeverhalten des nephelins in zwei vorkommen alkaliner kristaliner schiefer. *Bulletin of the Geological Institution of the University of Upsala*, **39**, 1–31.

Koark, H.J. (1968) Zu hülle, inhalt, gefüge und alter des alkaligesteinsvorkommen von Norra Kärr im südlichen mittelschweden. *Geologiska Föreningen i Stockholm Förhandlingar*, **91**, 159–184.

Kogarko, L.N., Lazutkina, L.N. and Romanchev, B.P. (1982) The origin of eudyalite mineralization. Translations from *Geokhimiya*, **10**, 1415–1432.

Kontak, D.J. and Corey, M. (1988) Metasomatic origin of spessartine-rich garnet in the South Mountain Batholith, Nova Scotia. *The Canadian Mineralogist*, **26**, 315–334.

Kornprobst, J., Cantagrel, J.-M., Fabriès, J., Lasserre, M., Rollet, M. and Soba, D. (1976) Existence, au Cameroun, d'un magmatisme alcalin panafricain ou plus ancien, la syénite néphélinique à mboziite de Nkonglong – comparison avec les roches alcalines connues dans la même region. *Bulletin de la Société Géologique de France*, **18**, 1295–1305.

Le Maitre, R.W. (2002) *Igneous Rocks: A Classification and Glossary of Terms.* Cambridge UP, UK.

Lumbers, S.B. (1976) Omphacite-bearing nepheline syenite in an anorthosite complex, Grenville, Province of Ontario. *Geological Association of Canada/Mineralogical Association of Canada Joint Annual Meeting, Program with Abstracts*, **1**, 73.

Mahato, A.C., Ren, M., Chakrabarty, A., Sen, A.K., Rajesh, H.M. and Shindo, K. (2013) Reconstruction of magmatic to deuteric stages of eudialyte-bearing Sushina syenite gneiss West Bengal, India. *Journal of Indian Geological Congress*, **5**, 77–93.

Maji, A.K., Goon, S., Bhattacharya, A., Mishra, B., Mahato, S. and Bernhardt, H.J. (2008) Proterozoic polyphase metamorphism in the Chhotanagpur Gneissic Complex (India), and implication for transcontinental Gondwanaland correlation. *Precambrian Research*, **162**, 385–402.

Markl, G. and Baumgartner, L. (2002) pH changes in peralkaline late-magmatic fluids. *Contributions to Mineralogy and Petrology*, **144**, 331–346.

Markl, G., Marks, M., Schwinn, G. and Sommer, S. (2001) Phase equilibrium constraints of intensive crystallization parameters of the Ilímaussaq Complex, South Greenland. *Journal of Petrology*, **42**, 2231–2258.

Markl, G., Marks, M.A.W. and Frost, B.R. (2010) On the controls of oxygen fugacity in the generation and crystallization of peralkaline melts. *Journal of Petrology*, **51**, 1831–1847.

Marks, M.A.W., Schilling, J., Coulson, I.M., Wenzel, T. and Markl, G. (2008) The alkaline-peralkaline Tamazeght complex, High Atlas Mountains, Morocco: mineral chemistry and petrological constraints for derivation from a compositionally heterogeneous mantle source. *Journal of Petrology*, **49**, 1097–1131.

Marks, M.A.W., Hettmann, K., Schilling, J., Frost, B.R. and Markl, G. (2011) The mineralogical diversity of alkaline igneous rocks: critical factors for the transition from miaskitic to agpaitic phase assemblages. *Journal of Petrology*, **52**, 439–455.

Mitchell, R.H. (1996) Classification of undersaturated and related alkaline rocks. Pp. 1–22 in: *Undersaturated Alkaline Rocks: Mineralogy, Petrogenesis, and Economic Potential* (R.H. Mitchell, editor). Short Couse, **24**, Mineralogical Association of Canada.

Mitchell, R.H. and Chakrabarty, A. (2011) *Peralkaline Nepheline Gneiss from Purulia, West Bengal, India: Paragenesis of a New Eudialyte Group Mineral.* PERALKCARB 2011. University of Tübingen, Germany (extended abstract), 100–102.

Mitchell, R.H. and Chakrabarty, A. (2012) Paragenesis and decomposition assemblage of a Mn-rich eudialyte from the Sushina peralkaline nepheline syenite gneiss, Paschim Bnaga, India. *Lithos*, **152**, 218–226.

Mitchell, R.H. and Liferovich, R.P. (2006) Subsolidus deuteric/hydrothermal alteration of eudialyte in lujavrite from the Pilansberg alkaline complex, South Africa. *Lithos*, **91**, 352–372.

Mogessie, A., Ettinger, K., Leake, B.E. and Tessardi, R. (2001) AMPH-IMA97: a hypercard program to determine the name of an amphibole from electron microprobe and wet chemical analyses. *Computers & Geosciences*, **27**, 1169–1178.

Nachit, H., Ibhi, A., Abia, E.H. and Ohoud, M.B. (2005) Discrimination between primary magmatic biotites,

https://doi.org/10.1180/minmag.2016.080.057 Published online by Cambridge University Press

reequilibrated biotites and neoformed biotites. *Comptes Rendus*, **337**, 1415–1420.

Olivo, G.R. and Williams-Jones, A.E. (1999) Hydrothermal REE-rich eudialyte from the Pilanesberg complex, South Africa. *The Canadian Mineralogist*, **37**, 653–663.

Perchuk, L.L. and Ryabchikov, I.D. (1968) Mineral equilibria in the system nepheline-alkali feldspar-plagioclase and their petrological significance. *Journal of Petrology*, **9**, 123–167.

Pfaff, K., Wenzel, T., Schilling, J., Marks, M. and Markl, G. (2010) A fast and easy-to-use approach to cation site assignment for eudialyte-group minerals. *Neues Jahrbuch für Mineralogie, Abhandlungen*, **187**, 69–81.

Platt, R.G. (1996) Nepheline syenite complexes: an overview. Pp. 63–99 in: *Undersaturated Alkaline Rocks: Mineralogy, Petrogenesis, and Economic Potential* (R.H. Mitchell, editor). Short Couse 24, Mineralogical Association of Canada.

Popp, R.K. and Gilbert, M.C. (1972) Stability of acmite-jadeite pyroxene at low pressure. *American Mineralogist*, **57**, 1210–1231.

Pouchou, J.L. and Pichoir, F. (1991) Quantitative analysis of homogeneous or stratified microvolumes applying the model "PAP". Pp. 31–75 in: *Electron Probe Quantitation* (K.F.J. Heinrich and D.E. Newbury, editors). Plenum Press, New York.

Ratschbacher, B.C., Marks, M.A.W., Bons, P.D., Wenzel, T. and Markl, G. (2015) Emplacement and geochemical evolution of highly evolved syenites investigated by a combined structural and geochemical field study: the lujavrites of the Ilímaussaq complex, SW Greenland. *Lithos*, **231**, 62–76.

Reider, M., Cavazzini, G., D'Yakonov, Y.S., Frank-kamenetskii, V.A., Gottardi, G., Guggenheim, S., Koval, P.V., Muller, G., Neiva, A.M.R., Radoslovich, E.W., *et al.* (1998) Nomenclature of the micas. *The Canadian Mineralogist*, **36**, 905–912.

Rekha, S., Upadhyay, D., Bhattacharya, A., Kooijman, E., Goon, S., Mahato, S. and Pant, N.C. (2011) Lithostructural and chronological constraints for tectonic restoration of Proterozoic accretion in the Eastern Indian Precambrian shield. *Precambrian Research*, **187**, 313–333.

Robertson, E.C., Birch, F. and Macdonald, G.J.F. (1957) Experimental determination of jadeite stability relations to 25,000 bars. *American Journal of Science*, **255**, 115–137.

Saha, A.K. (1994) *Crustal Evolution of Singhbhum-North Orissa, Eastern India.* Memoir Geological Society of India, **27**, 341.

Salvi, S. and Williams-Jones, A.E. (1995) Zirconosilicate phase relations in the Strange Lake (Lac Brisson) pluton Quebec – Labrador, Canada. *American Mineralogist*, **80**, 1031–1040.

Sanyal, S. and Sengupta, P. (2012) Metamorphic evolution of the Chotanagpur Granite Gneiss Complex of East Indian Shield: current status. Pp. 117–145 in: *Palaeoproterozoic of India* (R. Mazumder and D. Saha, editors). Special Publications **365**, Geological Society, London.

Schilling, J., Wu, F.-Y., McCammon, C., Wenzel, T., Marks, M.A.W., Pfaff, K., Jacob, D.E. and Markl, G. (2011*a*) The compositional variability of eudialyte-group minerals. *Mineralogical Magazine*, **75**, 87–115.

Schilling, J., Marks, M.A.W., Wenzel, T., Vennemann, T., Horvath, L., Tarassoff, P., Jacob, D.E. and Markl, G. (2011*b*) The magmatic to hydrothermal evolution of the intrusive Mont Saint-Hilaire complex: insights into the late-stage evolution of peralkaline rocks. *Journal of Petrology*, **52**, 2147–2185.

Schönenberger, J. and Markl, G. (2008) The magmatic and fluid evolution of the Motzfeldt intrusion in South Greenland: insights into the formation of agpaitic and miaskitic rocks. *Journal of Petrology*, **49**, 1549–1577.

Sheard, E.R., Williams-Jones, A.E., Heiligmann, M., Pederson, C. and Trueman, D.L. (2012) Controls on the concentration of zirconium, niobium, and the rare earth elements in the Thor Lake Rare Metal Deposit, Northwest Territories, Canada. *Economic Geology*, **107**, 81–104.

Sjöqvist, A.S.L., Cornell, D.H., Andersen, T., Erambert, M., Ek, M. and Leijd, M. (2013) Three compositional varieties of rare-earth element ore: eudialyte-group minerals from the Norra Kärr Alkaline Complex, Southern Sweden. *Minerals*, **3**, 94–120.

Sørensen, H. (1992) Agpaitic nepheline syenites: a potential of rare elements. *Applied Geochemistry*, **7**, 417–427.

Sørensen, H. (1997) The agpaitic rocks – an overview. *Mineralogical Magazine*, **61**, 485–498.

Tilley, C.E. (1954) Nepheline-alkali feldspar paragenesis. *American Journal of Science*, **252**, 65–75.

Tilley, C.E. (1957) Problems of alkali rock genesis. *13th William Smith Lecture*, 323–360.

Tindle, A.G. and Webb, P.C. (1990) Estimation of lithium contents in trioctahedral micas using microprobe data: application to micas from granitic rocks. *European Journal of Mineralogy*, **2**, 595–610.

Tischendorf, G., Förster, H.-J., Gottesmann, B. and Rieder, M. (2007) True and brittle micas: composition and solid-solution series. *Mineralogical Magazine*, **71**, 285–320.

Upadhyay, D. (2012) Alteration of plagioclase to nepheline in the Khariar alkaline complex, SE India: constraints on metasomatic replacement reaction mechanisms. *Lithos*, **155**, 19–29.

Ussing, N.V. (1912) Geology of the country around Julianehaab, Greenland. *Meddelelser om Grønland*, **38**, 1–376.

https://doi.org/10.1180/minmag.2016.080.057 Published online by Cambridge University Press

von Eckermann, H. (1968) New contributions to the interpretation of the genesis of the norra kärr alkaline body in southern Sweden. *Lithos*, **1**, 76–88.

Vuorinen, J.H., Hålenius, U., Whitehouse, M.J., Mansfeld, J. and Skelton, A.D.L. (2005) Compositional variations (major and trace elements) of clinopyroxene and Ti-andradite from pyroxenite, ijolite and nepheline syenite, Alnö Island, Sweden. *Lithos*, **81**, 55–77.

Woolley, A.R., Platt, R.G. and Eby, N.E. (1996) Relatively aluminous alkali pyroxene in nepheline syenites from Malawi: mineralogical response to metamorphism in alkaline rocks. *The Canadian Mineralogist*, **34**, 423–434.

Yoder, H.S. and Weir, C.E. (1951) Change of free energy with pressure of the reaction nepheline + albite = 2 jadeite. *American Journal of Science*, **249**, 683–694.

https://doi.org/10.1180/minmag.2016.080.057 Published online by Cambridge University Press